Experimental Study of Tool -Part Interaction during Autoclave Processing of Aerospace Thermoset Composite Structures

by

Vibhu Kaushik

A Thesis

Submitted to the Faculty of Graduate Studies

In Partial Fulfillment of the Requirements

For the Degree of

MASTER OF SCIENCE

Department of Mechanical & Manufacturing Engineering

University of Manitoba

THE UNIVERSITY OF MANITOBA

FACULTY OF GRADUATE STUDIES

*****

COPYRIGHT PERMISSION

Experimental Study of Tool-Part Interaction During Autoclave Processing of Aerospace Thermoset Composite Structures

BY

Vibhu Kaushik

A Thesis/Practicum submitted to the Faculty of Graduate Studies of The University of Manitoba in partial fulfillment of the requirement of the degree

Of

Master of Science

ABSTRACT

Autoclave processing of large and complex thermoset polymer composite structures is challenging due to process-induced warpage. One important contributor to the process-induced warpage is the interaction between the composite part and the tool on which the part is laid while being processed in an autoclave. Current level of understanding of this tool-part interaction is limited and hence, is the focus of this thesis. An experimental study was pursued to understand the tool-part interaction and its role in process-induced warpage of thermoset polymer composite structures. A friction test fixture, specially designed to simulate the autoclave environment, was used to measure the static (μ_{static}) and dynamic ($\mu_{dynamic}$) friction coefficients at various time intervals during autoclave processing. Both friction coefficients varied with process time. From a maximum value at the start of the process cycle for an uncured composite with zero degree of cure ($\alpha = 0$), the μ_{static} decreased with an increase in process time until the composite's viscosity reached a minimum when the degree of cure (α) was 0.2. Subsequently, α magnitude increased until gelation ($\alpha = 0.4$) beyond which it decreased again until $\alpha = 0.6$. Between $\alpha = 0.6$ and 1.0, the μ_{static} increased again though the value at $\alpha = 1.0$ was less than the value at $\alpha = 0$. In contrast to this trend, the $\mu_{dynamic}$ decreased continually with an increase in process time and α. When the above test was repeated for another autoclave process cycle with a higher ramp rate, the magnitudes of the μ_{static} were the same for both ramp rates (3 °F/min and 2 °F/min) until $\alpha = 0.4$, beyond which they differed significantly. Based on this observation as well as fractographic examination of the tool surface, after testing, it was concluded that the friction coefficients changed with process time and

cycle due to a continually changing tool-part interface, composite properties, and process-induced residual stress. These friction coefficient values were used in an ABAQUS-based 3D process model developed by the other members of the Composite Materials and Structures Research Group to model the tool-part interaction during processing, resulting in realistic predictions of process-induced warpage in a large composite structure of an aircraft.

ACKNOWLEDGEMENTS

Thanks to fellow members of the 'Composite Materials & Structures Research Group' for their encouragement & support. Special thanks to:

- Anand Birur for his support in my initial learning to work with Instron apparatus and Data Acquisition System (DAQ).
- David Bonin, Yang and Mahi for their support with Differential Scanning Calorimeter (DSC) experiments.

Many thanks to the employees of the project partners:

- Loren Hendrickson for his support and advice regarding the tool-part experiments.
- R. Mark Shead for his help in doing PLC controller calibration to simulate the thermal environment in tool-part apparatus.

Additional Thanks to:

- John Van Dorp & Mike Boskwick, Technicians with the Department of Mechanical Engineering and Manufacturing Engineering at University of Manitoba for their help in mounting and removing the apparatus several times on the Instron as needed, load cell installations and providing the accessories for experiments.

Thanks to NSERC, Boeing Canada Technology, Winnipeg Division and the University of Manitoba for their financial support for the project.

Very special thanks to:

- Dr. Raghavan Jayaraman, my advisor, for his support and advice throughout the project and the thesis work.
- Dr. Neil Popplewell and Dr. Michael Freund, my examining committee members.
- My family and friends for their words of encouragement & continuous support.

TABLE OF CONTENTS

Page Number

CHAPTER 3 – EXPERIMENTAL DETAILS

CHAPTER 4 – RESULTS & DISCUSSION

CHAPTER 5 – CONCLUSIONS

LIST OF FIGURES

LIST OF TABLES

NOMENCLATURE

Variable	Description	Units
T	Temperature	°F
ΔT	Temperature difference	°F
N	Normal force	N
F_{static}	Static force	N
$F_{dynamic}$	Dynamic force	N
CTE	Coefficient of thermal expansion	/ °F
ΔCTE	Difference in CTE	/ °F
α	Degree of cure	---
μ_{static}	Static friction coefficient	---
$\mu_{dynamic}$	Dynamic friction coefficient	---

CHAPTER 1

INTRODUCTION AND BACKGROUND

1.0 Introduction

Advanced composites utilizing glass or carbon fibers are widely used in both the aerospace and transportation industries owing to weight and cost advantages over traditional metals. Other advantages include better fatigue and corrosion resistance and manufacturing flexibility. These advanced composite materials are increasingly used in the aerospace, automotive, ground transportation, infrastructure and sporting goods industries. In civil aircraft applications, the share of polymer composites has increased from 10-12 % of the structural weight to about 21% in the recently introduced Airbus 380 and to about 50% in the Boeing 787.

1.1 Autoclave Processing

Aerospace thermoset composites are typically manufactured in an autoclave, under heat and pressure. Figure 1.1 shows a photograph of a typical autoclave used for the processing of composites. The uncured composite prepreg plies, consisting of a single layer of parallel or woven high modulus fibers impregnated with resin, are cut, stacked on a tool, and shaped to form the desired structure. This process is called the lay-up process. The plies are stacked on top of each other with the fibers in them oriented in pre-determined directions to form a laminate lay-up sequence that would yield desired mechanical properties. These stacked plies are vacuum bagged and then loaded into the autoclave, as shown in Figure 1.2. The purpose of the vacuum bag is two-fold. Firstly, it

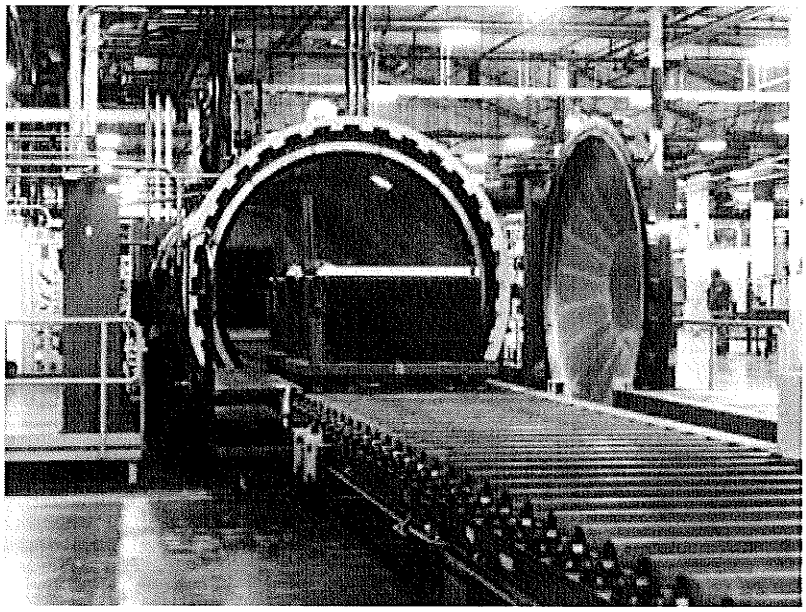

Figure 1.1: Photograph of a typical autoclave used in manufacturing composite structures

(Courtesy: - Thermal Equipments Ltd.)

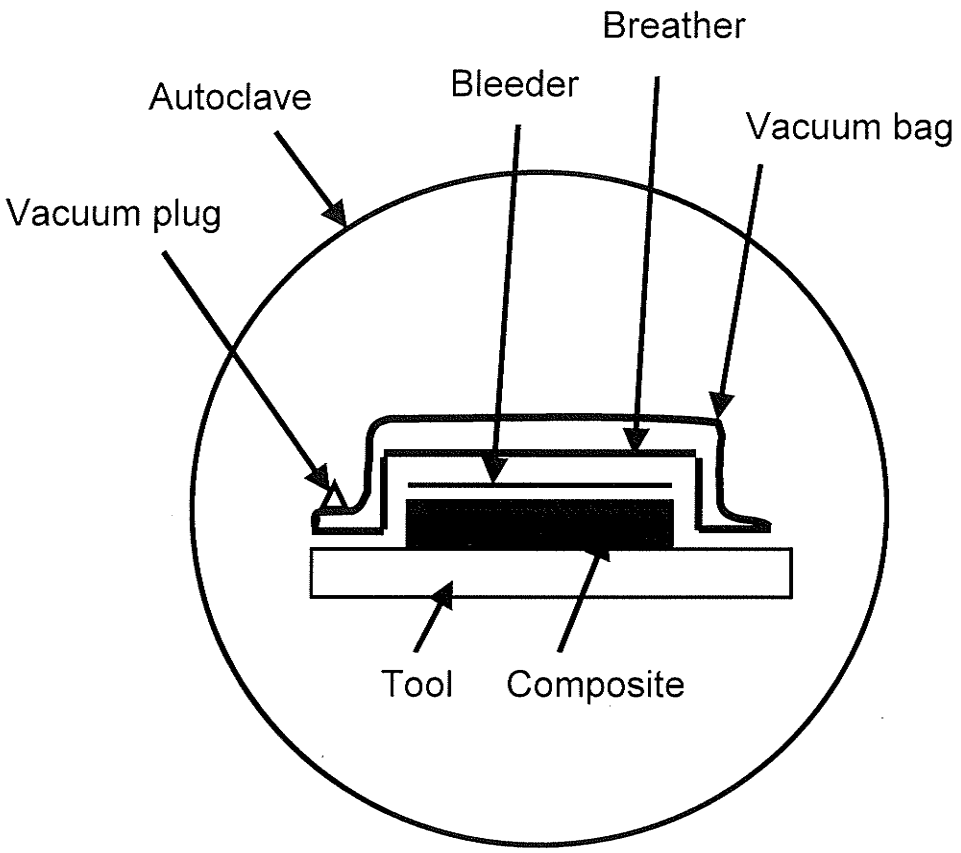

Figure 1.2: Schematic of composite and tool assembly in an autoclave

enables application of compaction pressure to the laminate, which is equal to the differential pressure between the pressure inside the vacuum bag and the autoclave pressure. During the initial parts of the cure cycle, the pressure within the vacuum bag will be -101.3 kPa (-14.7 psi). Aided by this pressure, the resin flows which results in compaction to yield a quality laminate. Secondly, the vacuum bag aids in the extraction of moisture and solvents dissolved in the polymer matrix of the composite and volatiles generated curing composite, lest they would get entrapped in the laminate as voids.

Figure 1.3 shows a typical temperature and pressure cycle used in autoclave processing for manufacturing aerospace composite structures. A typical pressure value of 45 psi is commonly used in the aerospace industry for parts with honeycomb cores. The temperature cycle has three components; a ramp up component during which the temperature increases at a constant ramp rate, an isothermal component where the temperature stays constant, and a ramp down component during which the temperature decreases at a constant ramp rate. During the initial portion of the cure cycle the pressure inside the vacuum bag is -101.3 kPa, and hence, the differential pressure acting on the laminate will be 59.7 psi (45 + 14.7). At a pre-determined time, the vacuum bag is vented to atmosphere when the differential pressure will be 30.3 psi (45 - 14.7). During the ramp-up portion of the autoclave cure cycle, the thermoset matrix resin flows due to a decrease in viscosity, under the compaction pressure resulting in the consolidation of the composite. Subsequently, the resin cures (i.e. polymerizes and cross-links) during the isothermal hold period of the cure cycle, transforming the semi-solid composite into a

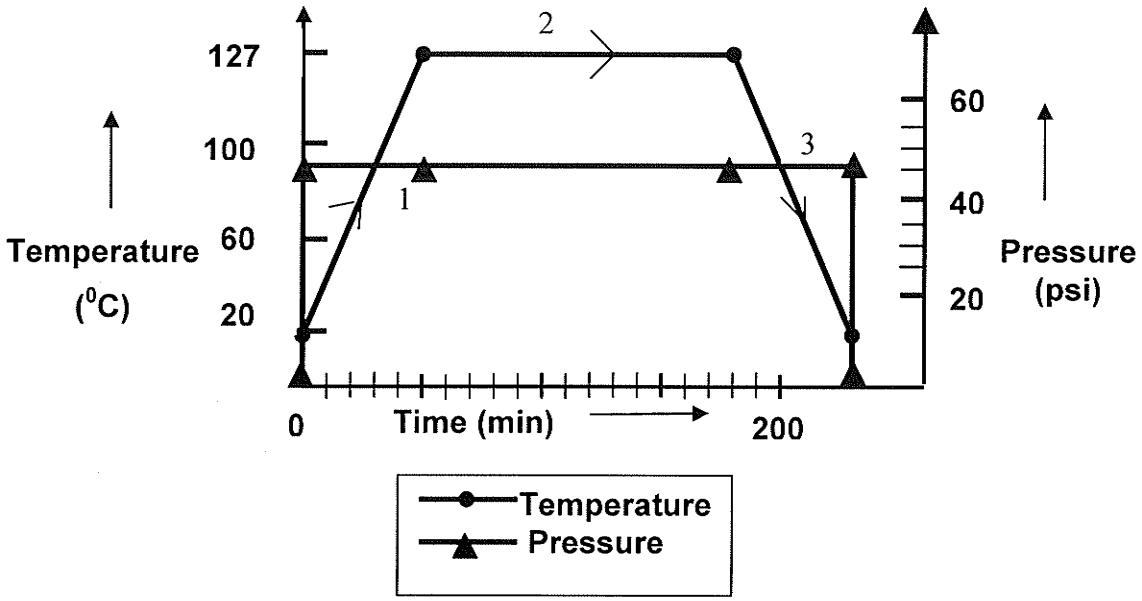

Figure 1.3: A typical temperature/pressure cure cycle (Courtesy: - Cytec fiberite manufacturer data sheet)

solid. Subsequently, the autoclave is ramped down, pressure is released, and the cured laminate is removed from the vacuum bag. The dimensions of the cured composite often deviate from the original values and this is known as *warpage*. As shown in Figure 1.4 the angle laminate is designed to have a nominal right angle. However, due to process induced warpage a reduction in the included angle can be observed [3-4]. Process induced warpage is an important issue in an application that requires an accurate tolerance. Normally, the parts are force fitted due to this warpage (provided the fitting force is within accepted limits) else the part is rejected. Since these parts are very costly, minimization of warpage is highly desired. Hence, understanding process-induced warpage and minimizing it is very important during autoclave manufacturing of polymer composite structures. During the past two decades, substantial effort in this area has been expended by researchers around the world. Good reviews can be found in references [1] to [8]. Based on the past efforts, Koteshwara [1] categorized the various contributors to process-induced warpage as shown in Figure 1.5

One major contributor is the anisotropy in thermoset prepreg's CTE (Coefficient of Thermal Expansion) and cure shrinkage coefficient. CTE of the fibers are generally lower than that of the polymer matrix. Additionally, the polymer resin shrinks during the curing process while the fiber does not under go any change. Hence, the fibers prevent thermal expansion or contraction of the resin during ramp-up and ramp-down of the cure cycle as well as contraction of the resin due to cure shrinkage. This constraint will be more in the direction parallel to the fiber axis and less in the direction transverse to the fiber axis resulting in residual stresses. While this anisotropy does not lead to warpage in flat parts,

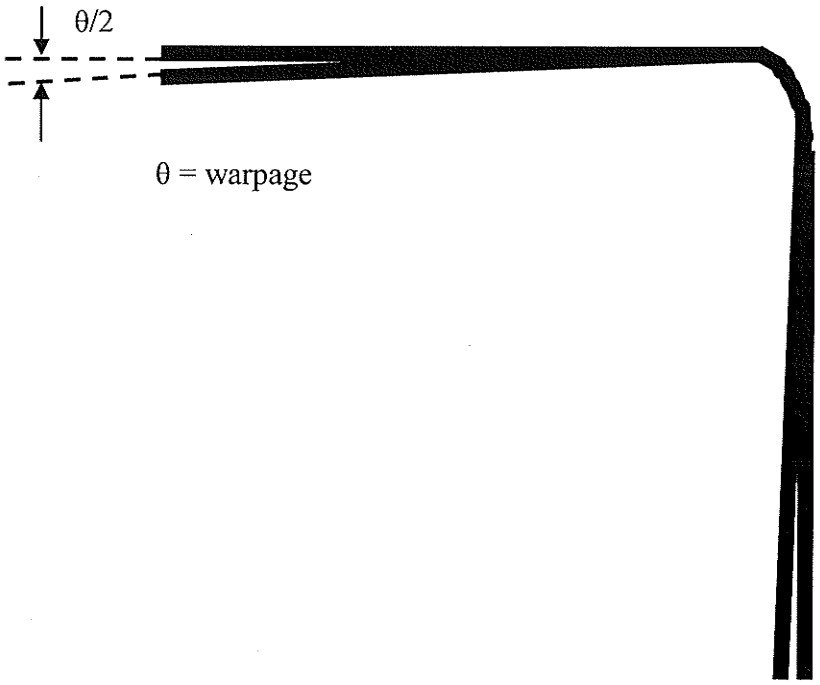

Figure 1.4: Reduction in included angle of an angled laminate due to process-induced warpage

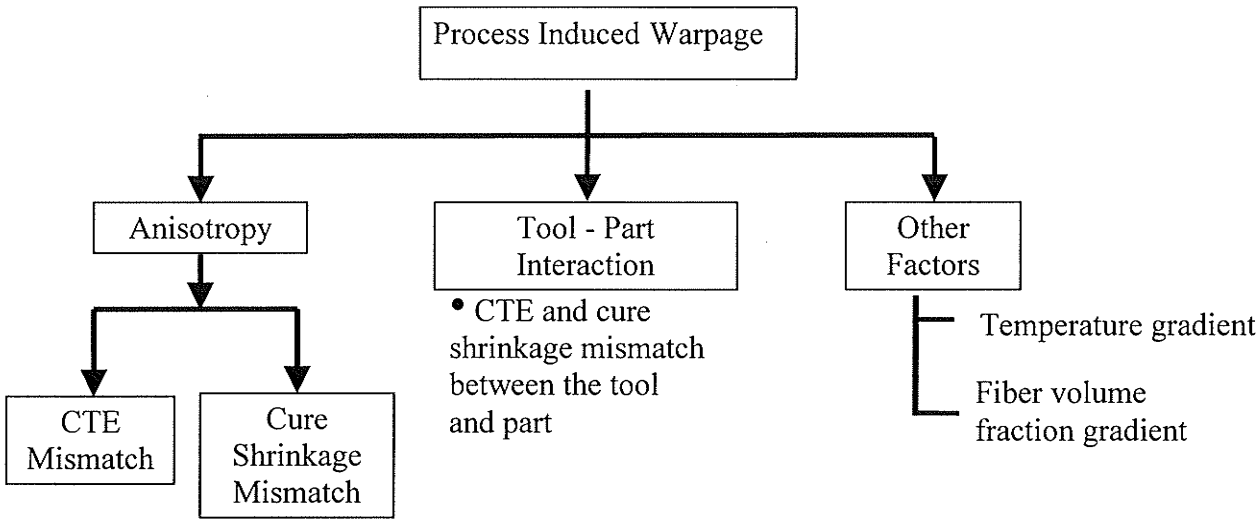

Figure 1.5: Mechanisms causing process induced warpage in composite structures

it does in parts with a curvature due to difference in mismatch in CTE and cure shrinkage coefficient between the in-plane and out-of plane directions. A second possible contributor is the gradient in temperature and fiber volume fraction within the laminate due to uneven resin flow. Since the likelihood of encountering this behavior in thin composite structures is small, most previous studies did not focus on this aspect. A third contributor is the tool-part interaction, which can lead to warping even in flat laminates.

1.2 A Primer on Tool-Part Interaction

The mechanism of tool-part interaction can be understood using a one-dimensional illustration. Consider a single layer of uni-directional composite lamina laid on a thin metallic tool. It is assumed that (i) the stiffness of the tool is comparable to that of the part and (ii) the interface between the tool and the part does not change during processing. Due to orientation of the fibers along the length direction, the CTE of the lamina will be much less than that of the metallic tool. When this tool-part assembly is subjected to an autoclave cure cycle, the differential expansions in the tool and the lamina will cause the tool and the part to warp concave up, during ramp-up, provided (a) there is no autoclave pressure, and (b) either both are bonded well or both have a frictional interface. Maximum curvature will be observed for a fully bonded condition. In the presence of autoclave pressure, the tool and the part will be prevented from warping, leading to a tensile stress in the composite lamina and compressive stress in the tool. The magnitude of these stresses will be proportional to ΔCTE and ΔT (T_{cure}-T_{room}) and the modulus of the tool and the part. Since the polymer matrix of the lamina can hardly support any load below the gel point and the lamina modulus begins to increase substantially with the

degree of cure only beyond gelation, the magnitude of tensile stress in the lamina during the ramp depends on the temperature at which the gelation occurs. Below gelation, the viscosity of the resin decreases with an increase in temperature and the resin flows easily without any ability to support a load. The fibers in the lamina may be stretched by the expanding tool. Hence, the tensile stress in the lamina when it reaches T_{cure} depends on the temperature at which gelation (T_{gel}) occurs during ramp-up. If the ramp-up rate is high, the gelation may not occur until after T_{cure} is reached and the tensile stress will be minimal. If the ramp rate is low, gelation will occur much before T_{cure}, resulting in a substantial tensile stress. At T_{cure}, the composite lamina cures further and hardens. Assume that there is no cure shrinkage strain. During ramp-down, compressive and tensile stresses will be introduced in the lamina and tool respectively, and their magnitudes will be proportional to ΔCTE and ΔT and the modulus of the tool and the lamina. If the composite modulus does not change during heating and cooling, the stresses in the tool and the part will be zero at the end of the cure cycle and hence, there will be no warpage of the part after removal from the tool. However, if the modulus changes, then the magnitude of the stresses introduced in the lamina and tool during ramp-up will be different from the magnitude of the stresses introduced during ramp-down, resulting in non-zero stress values. Since these stresses will be non-uniform across the thickness, the lamina will warp upon tool removal, as shown in Figure 1.6. Additionally, cure shrinkage strains can increase the magnitude of stresses in the lamina and the tool during ramp-up and hold at T_{cure}. The net stress values at the end of ramp-down will be higher due to cure shrinkage strains resulting in larger warpage.

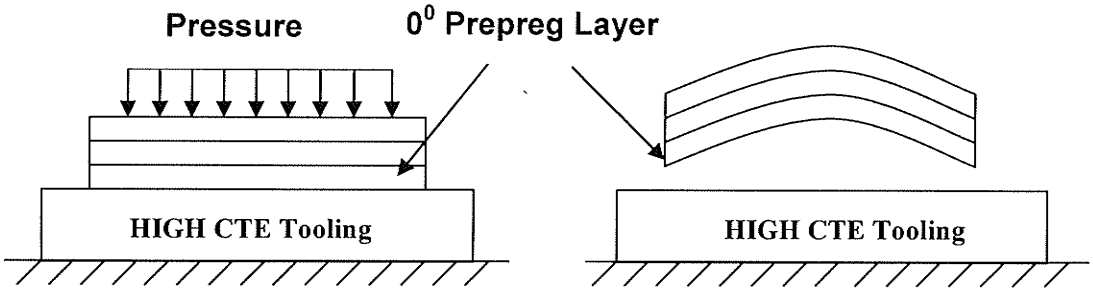

(a) During autoclave heat up (b) After cool down and separation

Figure 1.6: An illustration of tool-part interaction

If laminates are considered instead of a lamina, slippage can take place between the lamina layers. This can influence the final warpage by altering the stress distribution across the thicknesses of both the lamina and the laminate.

1.3 Motivation

In order to minimize this tool-part interaction, the tool-surfaces are coated currently with a non-stick coating. Despite this, warpage is observed in autoclave manufactured structures pointing to the existence of a substantial tool-part interaction. Published studies on tool-part interaction are very limited and mostly focused on experimental correlation of various experimental factors to warpage for simple shapes [9-14]. However, further research is required to understand this better and quantify it. The latter is required for use in a process model for prediction and minimization of process-induced warpage. This is the motivation for this study.

1.4 Scope of this Thesis

The scope of this thesis is to experimentally quantify the tool-part interaction by measuring the friction coefficients between the tool and the part during autoclave processing and delineate the various influencing factors.

1.5 Thesis Outline

Background on process induced warpage and autoclave processing along with a brief outline of relevance of tool-part interaction, its theoretical background and scope of this thesis has been provided in Chapter 1. A thorough review of the published literature on

tool-part interaction is provided in Chapter 2. Chapter 3 presents details on the experimental setup. Chapter 4 presents the results and discussions along with a detailed error analysis done to compute the errors in magnitudes of degree of cure and friction coefficients. The conclusions drawn from this work are provided in Chapter 5 along with recommendations for future work.

CHAPTER 2

LITERATURE REVIEW AND OBJECTIVES

2.0 Introduction

At the outset, a brief summary of the published literature in the area of process-induced residual stress and warpage in composite structures is presented. Following this, published literature in the area of tool-part interaction is reviewed. Finally, the various factors influencing the tool-part interaction are listed and objectives of this thesis are presented.

2.1 Published Work on Process-induced Stress and Warpage

While a detailed literature review on process-induced stress and warpage is beyond the scope of this thesis, a few representative studies are highlighted here.

The contribution of anisotropy in process induced warpage has been extensively studied by several researchers. Jain and Mai [3, 4] performed both an experimental and analytical study of process induced warpage in composite laminates. They studied the effect of tool material, tool geometry, lay-up sequence and ply orientation on the process induced warpage. A summary of this parametric study is given in Table 2.1. Since they did not consider tool-part interaction, and the gradient in temperature, cure and fiber volume fraction, their results could be considered to be indicative of the contribution of the anisotropy in CTE and cure shrinkage to warpage. They concluded that,

- The effect of tool material on process induced warpage was insignificant in

Table 2.1: Summary of experimental and simulation parametric study [3-4]

Parameter	**Variation from nominal value**	**Effect on warpage (Angle)**	**Case study & Nature of study**
Ply sequence for symmetric laminate	$[90/0/90/0]_s$	1.23	Angle laminate Experimental and Analytical
	$[0/90/0/90]_s$	1.2	
Tool material	Aluminum	1.39	
	Steel	1.34	
	Composite	1.45	
Tool Angle (degrees)	45	2.09	
	70	2.05	
	90	1.39	
	135	0.78	
Radius/Thickness (R/h)	0-20	1.4	

contrast to the results of references 11, 12 and 20.

- In the case of curved composite structures, the spring back decreased with increase in tool angle.
- The effect of tool radius to part thickness ratio was not significant in the case of angle laminates.
- In the case of symmetric laminates, the warpage was independent of laminate sequence.
- In the case of fabric laminates, the process-induced warpage was independent of the orientation angles.

In the prediction of process-induced warpage they used the cured composite mechanical properties. However, they did not study the continuous evolution of the mechanical properties during the cure cycle in their warpage predictions.

Sarranzin et. al. [5] performed an experimental parametric study of the process-induced deformation in flat laminates. They studied the effect of process and lay-up parameters on the process-induced warpage. The results of this study are summarized in Table 2.2. Their conclusions are given below.

- The process-induced warpage increased with increase in cure temperature.
- The warpage increased with degree of cure.
- The two step cure cycle reduced the warpage, in contrast to the conclusions given in references 11 and 12.
- The process induced deformation decreased with a decrease in cooling rate.
- The effect of cure pressure on process-induced warpage was negligible.

Table 2.2: Summary of experimental parametric study [16]

Parameter	**Variation from nominal value**	**Effect on warpage (ΔL/L)**	**Case study and Nature of study**
Cure T	Nominal	0.16	Flat laminate Experimental
	-15 %	0.1	
	+15 %	0.24	
Cure cycle Pressure	Applied	Negligible	
	Removed		
	After 70% cure		
Cooling rate	7.5 °F/min	0.25	
	1 °F/min	0.2	
Tool	Aluminum	0.15	
	Ceramic	0.15	
Teflon	Porous	0.23	
	Non-porous	0.22	
Part thickness	1	0.74	
$[0_n/90_n]$, n	2	0.24	
	4	0.05	
	8	0.0	
Stacking sequence	$[0/90]_4$	0.0	
	$[0_2/90_2]_2$	0.005	
	$[0_4/90_4]_t$	0.04	

- The influence of the arrangement of porous or non-porous Teflon on process-induced deformation was insignificant.
- The warpage was found to decrease with an increase in laminate thickness.

In this study the above experimental observations were made using a case study of flat laminates. However, the reasons for the above trend in process-induced warpage were not studied and explained. In addition, the above conclusions on process-induced warpage were derived based on the case study of flat laminates without considering the contribution of various mechanisms on process-induced warpage.

Another previous study [6] assumed that the warpage developed in the composite structures during processing was due to a mismatch in the Coefficient of Thermal Expansion (CTE) between various plies in laminate and between the composite and the tool. The previously described studies interpolated the warpage in terms of anisotropy in CTE and experimental parameters. However anisotropy in cure shrinkage or other mechanisms discussed in chapter 1 were not considered. Subsequent studies by Loos and Springer [7], Bogetti and Gillespie [8] and White and Hahn [9, 10] showed that the warpage in autoclave-cured composites is much more complex than discussed in the above simplified cases. They showed that the warpage was a coupled effect of multi-physical phenomena such as heat transfer, chemical cure kinetics, resin flow through a porous medium, void generation and thermal stress development.

A second cause discussed in Chapter 1 is due to one or more of the following:- uneven temperature distribution, uneven resin flow, gradient in the fiber volume fraction and

CTE within the part. In autoclave curing of composite laminates, a bleeder may be used on the top surface and near the edges to bleed out excess resin from the laminate. During this process, more resin may bleed out from the top plies of the composite than from the plies close to the tool surface. This would result in uneven resin flow causing a variation in CTE and a fiber volume fraction variation within the composite part. The top plies with a less resin will experience less cure shrinkage than the plies close to the tool with higher resin content. This gradient within the part would result in warping of the part as mentioned in the reference 11.

Mike et. al. [12] observed that heat transfer within the autoclave varied along the length of the autoclave as well as with the orientation of the composite parts with the free-stream within the autoclave. Such an uneven temperature distribution within the autoclave and variation in the heat transfer within the autoclave might result in an uneven temperature distribution and hence, an uneven degree of cure within the part. In thick composite laminates, a large temperature gradient has been observed due to large amounts of exothermic heat [13-14].

The above studies did not consider the third important cause, the tool-part interaction.

2.2 Previously Published Work on Tool-Part Interaction

Published research on tool-part interaction is limited and it is summarized in Table 2.3. A majority of references draws indirect inference on the interaction by studying experimentally the influence of various factors on observed warpage. Cann and Adams

[15] experimentally studied the cure-induced distortion of flat composite laminates due to both tool-part interaction effects and a through the thickness resin volume fraction gradient. They studied the effect of tool material, tool surface roughness, ply thickness and ply orientation on process-induced warpage. They concluded the following,

- The tool-material's CTE had a strong effect on the magnitude of distortion.
- Part thickness had significant influence on laminate distortion with thinner parts showing much greater curvature for the same tooling material and surface roughness.
- Ply orientation was found to have a significant impact on process-induced warpage. Specimens with 0^{o} plies adjacent to the tool showed a significant curvature where as the specimen with 90^{o} plies adjacent to the tool showed near zero curvature.
- Tooling surface roughness was found to have negligible effect on laminate distortion.

This study focused on process-induced warpage due to the tool-part interaction. They concluded that tool-part interaction is an important factor in producing the process-induced warpage and must be accounted for in the predictive model. However, they did not attempt to develop a predictive model based on their study.

Pagliuso [17], Nelson and Cairns [18] and Ridgard [19] demonstrated the significance of tool-part interaction and its role in process induced warpage in sandwiched panels in angled and flat laminates. Fernlund & Poursartip [20] performed the experimental and simulation parametric study of process-induced warpage in a C-channel composite

Table 2.3: Summary of previously published work on tool-part interaction

Reference	Work Done
Koteshwara et. al.[1-2], Jain et. al.[3-4]	Process induced warpage and various factors that contribute to it
Cann & Adams [15]	Experimentally studied cure-induced distortion of flat composite laminates, varied: part thickness, ply orientation, tool material & tool surface roughness
Pagliuso [17], Nelson & Cairns [18], Rigard [19]	Significance of tool-part interaction & its role in process induced warpage in flat laminates [18] and angled laminates [17]
Twigg et. al [21-23]	Strain induced in the part due to tool-part interaction measured using strain gauges
Johnston et. al. [24-26]	Used shear layer to account for tool-part interaction. However they calibrated its modulus using warpage data
Flanagan [27-28]	Quantified tool-part interaction by measuring friction coefficients between tool and part and between the plies as a function of autoclave temperature. Concluded that μ changes with tool surface preparation, fiber orientation and temperature

structure. They studied the influence of cure cycle and tool surface finish on process-induced warpage. From their study a trend in the process-induced warpage was not observed for the case of cure cycles with and without dwell. In addition, a trend was not observed for a tool surface finish. Besides, the predicted warpage using a process model was about 20% higher than the measured process-induced warpage. This could be due to the use of a calibrated shear layer for tool-part interaction and lack of knowledge of the contribution of tool-part interaction on process-induced warpage.

Twigg et. al. [21] – [23] experimentally studied the effect of process conditions and part aspect ratio on tool-part interaction induced warpage. They studied the effect of part length, part thickness, autoclave pressure, tool surface and specimen variability on the process induced warpage. Their study concluded the following,

- Longer parts were observed to warp considerably more than shorter parts, regardless of the process conditions or part thickness
- Thinner parts were observed to warp considerably more than thick parts for all part lengths and process conditions
- Warpage decreased with decrease in autoclave pressure for all except one data part which showed an opposite trend
- There was no predictable tool surface effect

They concluded that part aspect ratio had a much greater influence on warpage than the process conditions. Outcomes of their work were embodied in an empirical relation, which provided a guide to predict warpage over various conditions.

Johnston et. al. [24] – [26] performed a sensitivity analysis of the process-induced warpage in angle laminates and J-stiffened structures. The summary of this parametric study is provided in Table 2.4. They studied the effect of thermophysical properties, mechanical properties and initial and boundary conditions on process-induced warpage. However they assumed a thin imaginary shear layer between the tool and the part to represent a tool-part interaction. This study concluded the following,

- The predicted warpage is insensitive to the thermophysical properties of the composite
- The cure kinetics parameters and initial degree of cure plays an important role in the prediction of warpage
- The predicted warpage is very sensitive to the modulus of the composite and the modulus of the shear layer used to represent the tool-part interaction.

However, they also calibrated the shear modulus of this shear layer to match the measured warpage value with the predicted values.

Jose and Radford [12] studied the phenomenon of tool-part interaction experimentally through flat laminates as well as using a model. They studied the influence of various mold release agents and different tool material on process-induced warpage. In their model they used one coefficient (C_1) for tool-part interaction in the calculation of non-thermoelastic component of the induced strain of the sub layer closet to the tool, which is given by,

$$\varepsilon^{s(t)} = C_1(\varepsilon_t^T - \varepsilon_f^T) \tag{2.1}$$

where,

Table 2.4: Summary of simulation parametric study [24-26]

Parameter	**Variation from nominal value**	**Effect on warpage (Angle/Deflection)**	**Case study and Nature of study**
Analysis Parameter			Angle laminate and J-stiffened structure Simulation
Maximum overall time step (s) and degree of cure step	± 30% ± 50%	Negligible	
Thermophysical Properties			
C_p, k and V_f	± 10%	Insignificant	
Cure Kinetics Model			
Heat of reaction Cure kinetics	± 10%	Insignificant Significant	
Mechanical Properties			
Resin modulus developmet Cure shrinkage and composite CTE	± 10%	Significant Negligible	
Initial & Boundary Conditions			
Initial degree of cure Heat transfer coefficient	± 10%	Significant	
Process Cycle			
Process cycle		Insignificant	

$\varepsilon^{s(t)}$ is the non-thermoelastic component of the induced longitudinal strain in the sub-layer

C_1 is the coefficient of tool-part interaction

ε_t^T is the thermal strain in the tool

ε_t^T is the thermal strain of the fiber of the layer closest to the tool

The other coefficient (C_2) for the ply-to-ply interaction was used in the calculation of the non-thermoelastic component of the induced strain due to fiber-to-fiber interaction. It is given by,

$$\varepsilon_1^{sk} = C_2 \varepsilon_1^{sk+1} \tag{2.2}$$

Where,

ε_1^{sk} is the non-thermoelastic of the induced longitudinal strain in the sub-layer sk

C_2 is coefficient of interaction between sub-layers

ε_1^{sk+1} is the non-thermoelastic of the induced longitudinal strain in the sub-layer sk + 1

They assumed C_1 to be a function of the mold release agent, tool material and applied pressure. C_2 was assumed to be the function of applied pressure only. Similar to Johnston et. al. [24-26] values of C_1 and C_2 were obtained by fitting the experimental data with their model. They concluded that it is necessary to develop an experimental procedure to generate values of C_1 and C_2 related to various process conditions if this model is to be applied in commercial composite design. However the predictive capability of the approach used by Johnston et. al. [24-26], and Jose and Radford [12] was not satisfactory. The above literature emphasizes the contribution of tool-part interaction in warpage but

fails to exactly quantify its role, which is important for any reliable prediction of process induced warpage.

Flanagan [27-28] was the first to quantify tool-part interaction for thermoset composites. He measured the coefficient of friction between the tool and the part and between the plies assuming classical friction conditions using the Coulomb's friction model and a dry friction contact. As previously discussed in Chapter 1 the autoclave pressure which is required to force any volatilities out of the resin during the cure as well as to aid ply compaction, causes a large normal force to be exerted on the laminate stack, thus causing all the plies to come together. Hence, it is debatable as to what extent pure dry friction exists between the plies as opposed to a lubricated frictional interface through the resin interlayer. Flanagan demonstrated that there is some degree of contact between the adjacent fibers and the tool surface using an image magnified 2000 times. His research assumed that all the normal force acts on these interface fibers. Some of the other assumption he used in his analysis were:

- each ply was treated as a homologous fiber rich layer (volume fraction of fibers = 60%) with a fixed thickness
- the resin was considered to have no stiffness during the heat up period
- the plies became locked together the moment the autoclave temperature reached the cure temperature
- no temperature gradient existed in the laminate stack

- each ply through the stack was in direct contact with the plies above and below it, and the top ply was directly affected by the autoclave atmospheric pressure i.e. there was limited bulk modulus reaction from the resin
- the microscopic friction was equal to the macroscopic value

Flanagan applied the standard Coulomb friction model which assumes there is no relative motion between the interfaces if the equivalent friction stress is less than the critical stress, which is proportional to the contact pressure between them. When the equivalent friction force reaches the critical value then slip occurs. He used the tool-part friction coefficient (μ_1) and ply-ply friction coefficient (μ_2) in a model to predict the warpage. Then μ_1 was shown to be a more significant factor in its contribution towards the warpage than μ_2.

Flanagan measured μ_1 and μ_2 using a specially designed test rig. The test rig comprised of a hot plate, a universal tensile testing machine, a dead weight loading, thermocouple readings, displacement transducers (for interplay measurements), dial gauge (for interface ply measurements) and the carbon fiber ply. The universal tensile testing machine was used to produce a varying horizontal force. The normal force was provided by the dead weight loading which was altered to simulate different autoclave pressures. The temperature input was generated by the heated platen. The friction coefficients were measured as a function of temperature during the ramp up portion of the cure cycle. Flanagan concluded that the μ_1 varied with tool surface preparation, normal (autoclave) pressure, fiber orientation and temperature. Three sets of results were presented in his

work for μ_1; the frekote interface condition, the release film interface condition and the interplay condition.

However, this study did not offer any explanation for the variation of tool-part coefficient of friction with experimental parameters. Variations in μ_1 and μ_2 were studied for only the ramp up part of the cure cycle. In addition, the predicted warpage did not correlate well with the experimental results.

2.3 Summary of Literature Review and Motivation for This Thesis

The above review indicates that, while most studies have demonstrated indirectly the importance of tool-part interaction to process-induced warpage, Flanagan was the first person to study this effect directly and to quantify it. However, this study was not comprehensive. The tool-part interface is expected to change during autoclave processing due to flow, cure, and shrinkage of the resin matrix of the composite. The properties of the composite material at the interface will also change during processing. These factors will result in a continuous change in interfacial sliding of the part with respect to the tool and in the measured friction coefficients, during processing. Hence, the measurement of friction coefficients for typical autoclave cure cycles and an entire range of degree of cure is required to develop a comprehensive understanding of the tool-part interaction. Lack of this information in published literature is the motivation for this study.

2.4 Thesis Objectives

Based on the limitations of the published literature, the two key objectives of this research work are as follows:

1. Experimentally quantify tool-part interaction during the autoclave processing of aerospace thermoset composite structures by measuring the coefficient of friction between the tool and the part
2. Delineate the effect of various experimental factors on the coefficient of friction through a design of experiments (DOE) methodology

The various factors that have been identified to influence the tool-part interaction are:- (a) autoclave cure cycle, (b) misfit-strain between the surface of the tool and the part due to the roughness of the tool, and (c) tool-part interface area. This study was focused on factor (a). Factor (b) could be investigated with different surface coatings. In this study consistency was maintained by using three layers of the same coating material in all the experiments. Current experimental apparatus could not capture factor (c) as the area of available set of tool plates was the same. However this is an influencing factor and can be used for future work. While frictional slipping at the ply-ply interface may also affect process-induced warpage, it is beyond the scope of this thesis.

The various experimental parameters that can be varied to study the effect of autoclave cure cycle on friction coefficient at the tool – part interface are:

(a) degree of cure of the composite, which would alter the physical state of the composite from a uncured pre-preg to partially cured gel, to a fully cured state and influence the mechanical properties like the shear strength of the matrix at the interface

(b) temperature at the same degree of cure

(c) cure shrinkage

(d) ramp-up rate used to cure the composite to a particular degree of cure

The above factors were studied in this thesis.

CHAPTER 3

EXPERIMENTAL DETAILS

3.0 Introduction

The tool-part interaction is quantified in this study by measuring the friction coefficients. This chapter provides details on the experimental test fixture, material and test procedure used in this thesis to study and quantify tool-part interaction.

3.1 Measurement of Coefficient of Friction (μ)

Coefficient of friction (μ) was measured using a double shear experiment in which the sliding occurred at two tool-part interfaces. A free body diagram of the loading plate with the prepreg wrapped around it is shown in Figure 3.1. The loading plate was held stationary and attached to the load cell. The two tool plates applied a normal force (N) on both sides and were pulled down at a constant velocity. It was assumed that the contact between the tool plates and the prepreg wrapped around the loading plate was a surface contact and the normal force was applied uniformly on the surface. Once the tangential pull force (F/2) was greater than the friction force, sliding started on both the tool-part interfaces. Applying Coulomb's law as discussed in Appendix A, the coefficient of friction, independent of the test speed, was calculated as the ratio of the tangential reaction force of friction between the two bodies and the normal force pressing them together. Hence,

$$\mu = \frac{(\frac{F}{2})}{N} = \frac{F}{2N} \tag{3.1}$$

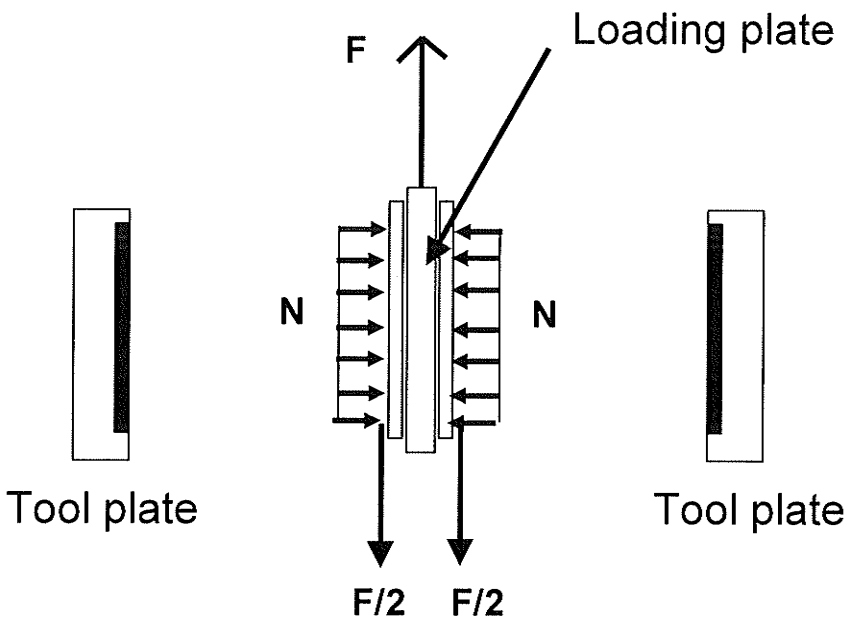

Figure 3.1: Free body diagram of the loading plate

3.2 Test Set-up

The double shear experiment discussed in the previous section was conducted using a special fixture, a schematic of which is shown in Figure 3.2. It consisted of two heated platens whose temperature was controlled using a Programmable Logic Controller (PLC) to simulate the autoclave temperature. One of the platens was stationary and the other was attached to a pneumatic ram. Two tool plates fixed to these platens sandwich the composite prepreg wrapped on the loading plate. The pneumatic ram pushed the moving tool plate and platen against the stationary tool plate and the platen to simulate the autoclave pressure. The air-pressure was adjusted to obtain the desired normal force on the composite.

Subsequent to the application of the normal force, the platens and the composite in contact with them were heated using the PLC controllers according to the programmed autoclave cure cycle (as shown later in Figure 3.5). Since the cooling of the platens could not be controlled, the cool-down part of the autoclave cure cycle was not controlled in this study. This did not impact the study since measurements were limited to the ramp-up and hold parts of the cure cycle only. The two heated tool plates and the loading plate have the same material and surface conditions as the actual tool used in the autoclave processing. Thus, the autoclave environment was simulated using this test fixture.

In order to measure the friction coefficient, the test fixture was mounted on the moving cross-head of the INSTRON's 8562 electro-servo test machine, as shown in Figure 3.3. The loading plate was connected to the stationary cross-head of the INSTRON and the

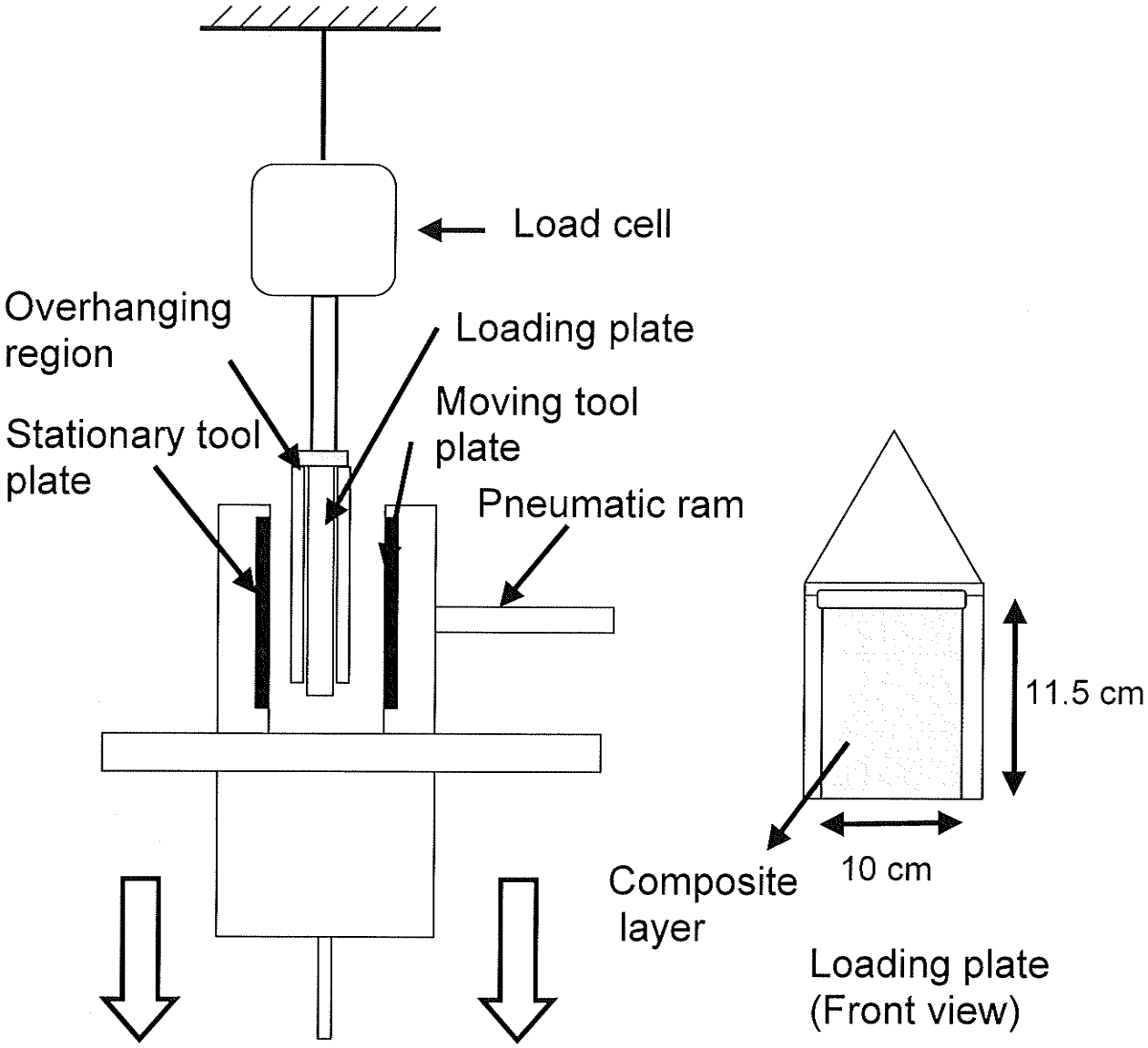

Figure 3.2: Schematic of the Test Fixture

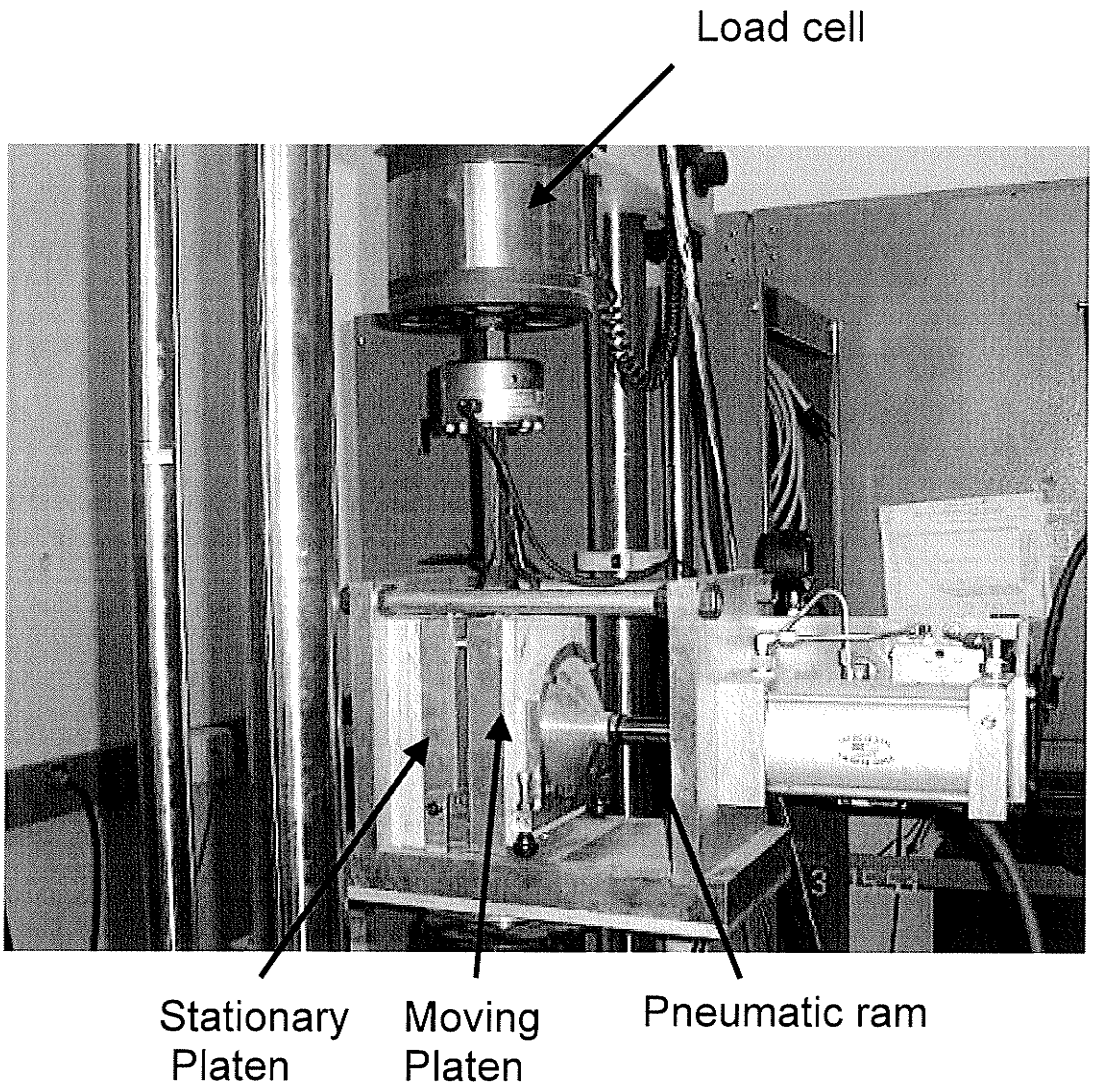

Figure 3.3: Picture of the test fixture

±25 kV load cell. When the moving cross-head was pulled down at a desired rate both the tool-plates, representing the tool, slid against the composite. The measured load corresponded to sliding over two tool-part surfaces.

3.2.1 Pressure

The normal pressure acting on the composite, pressing it against the tool plate, was determined by indicated shop air pressure multiplied by the load cylinder area (diameter 10 mm, area 0.0079 m^2) divided by the specimen area (0.0115 m^2). Thus, by varying the line air-pressure, the normal force was varied.

3.2.2 Temperature

The platens' temperature measured using a "J" type thermocouple, was used by the PLC controllers to control the temperature of the platens to a desired value.

3.2.2.1 Temperature variation across the tool-part interface

Multiple "J" type thermocouples were used to measure the temperature across the tool surface to verify the uniformity of temperature across the tool-part interface. The results are summarized in Figure 3.4. At the cure temperature of 260 ^{0}F, the maximum variation in temperature between the centre of interface area and the edges is about 5 ^{0}F. This difference can be attributed to heat loss from the edges to the ambient environment. Since the plate was heated across its entire area, it was assumed that the temperature gradient

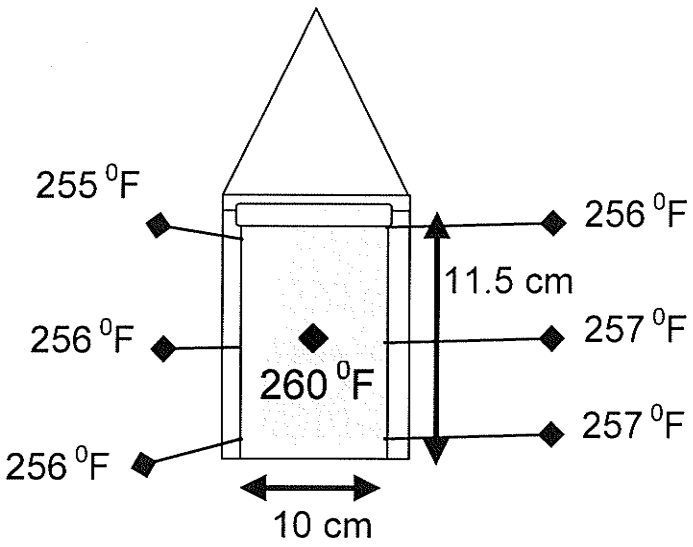

Figure 3.4: Variation of temperature on tool-part interface at the cure temperature (260 ^{0}F)

was limited to edges only and that the temperature was uniform across the major portion of the interface area.

3.3 Material

The material used was Cytec Fiberite's MXB7701-7781-B3 plain weave fabric of glass fiber impregnated with an epoxy matrix with a cure temperature of 127 °C (260 °F). The material was stored in a freezer in an air-tight bag. When required, the bag was taken out of the freezer and allowed to warm-up to ambient temperature. Subsequently, the material was taken out of the bag and used.

The cure kinetics of the Cytec MXB7701-7781-B3 resin was characterized by Bonin [29] using the TA instruments 2910 Differential Scanning Calorimeter (DSC). The material's cure reaction was found to be an autocatalytic reaction governed by the equation:

$$\frac{d\alpha}{dt} = k\alpha^n(1-\alpha)^m \tag{3.2}$$

where,

$\frac{d\alpha}{dt}$ is rate of change of degree of cure with respect to time

k is the rate constant and is defined by $k = ze^{(-\frac{Q}{RT})}$, where z is a pre-exponential factor, Q is activation energy, R is gas constant and T is temperature

α is degree of cure

m and n are constants

Table 3.1: Cure kinetics parameters for the Cytec MXB7701-7781-B3 [29]

Heat of Reaction	205.6 J/g
Activation Energy (Q)	75.89 kJ/mole
Pre-Exponential Factor (z)	9.138 (1/min)
Rate Constant (k)	$k = Z*\exp(-E/RT)$ $k(T) = 1.375E+09*\exp(-9127.99/T)$ [1/min] (T = Temperature in Kelvin)
N	$n(T) = 0.0163e^{0.039T}$ (T = Temperature in Celsius)
M	$m(T) = -0.0064T + 1.0397$ (T = Temperature in Celsius)

The experimentally determined constants of this material are tabulated in Table 3.1. These values were used in conjunction with equation 3.2 to determine the time to reach a desired degree of cure before completing a friction test.

3.4 Experimental Procedure

3.4.1 Surface Preparation

Prior to each test, the loading and tool plates were abraded with Scrotchbrite® and cleaned thoroughly with acetone to remove any residual resin and mold release. The plates were subsequently coated with three coats of Loctite® Frekote® NC710 with a 15 minute drying interval between two consecutive coats.

3.4.2 Test Coupon Preparation

Test coupons of dimensions 23 cm x 10 cm were cut from the pre-preg. A test coupon was wrapped around the loading plate to provide a tool-part interface area of 11.5 cm x 10 cm on each side. In case of tests involving multiple layers, one layer was applied at a time. Adequate hand pressure was applied to remove any noticeable air gaps between the first layer and the loading plate and between the two pre-preg layers.

3.4.3 Testing

In order to determine any possible lag in temperature between the programmed temperature and the actual platen temperature, calibration runs were done for programmed ramp rates of 3 ^{0}F/min and 2 ^{0}F/min under a 310.3 kPa (45 psi) clamping

pressure. The platens' actual face temperatures, measured using J type thermocouples, are plotted in Figures 3.5 and 3.6, respectively. The actual rate of heating of the tool surface was 2.90 ^{0}F/min when the programmed ramp rate was 3 ^{0}F/min and was 1.94 ^{0}F/min when the programmed ramp rate was 2 ^{0}F/min. The surface temperature calculated using actual surface ramp rates were used along with the cure kinetics parameters given in Table 3.2 to determine the degree of cure (α) at any given process time. A typical result is plotted in Figure 3.7 for a controller ramp rate of 3 ^{0}F/min. Even though the pre-pregs would have been minimally cured (B-staged) by the material supplier to a small extent (<5%) to enable easy handling, since this value is not known, the degree of cure in the as-received pre-preg was assumed to be zero for plotting and analysis. This plot was used to determine the time of heating to reach a desired degree of cure before the testing.

Once the desired degree of cure was reached, the specimen was pulled under tension by applying a cross-head rate of 15 mm/min. During the ramp-up to cure temperature sliding between tool and the part can occur due to the difference in CTE, provided there is no bonding between them. This can be estimated using equation 3.3.

$$\text{Sliding rate} = (\alpha_{Tool} - \alpha_{Composite}) \times \text{Ramp Rate} \times \text{Length of the composite} \quad (3.3)$$

Using representative values of α_{Tool} of 4.5E-05 /^{0}F, $\alpha_{Composite}$ of 1.5E-06 /^{0}F, composite length of 115 mm, the sliding rate for 3 ^{0}F/min and 2 ^{0}F/min are calculated to be 0.015 mm /min, and 0.010 mm/min respectively. During the isothermal hold period, the sliding would be due to cure shrinkage only. Hence, the sliding rate if the tool debonds from the part would be much less then the above values.

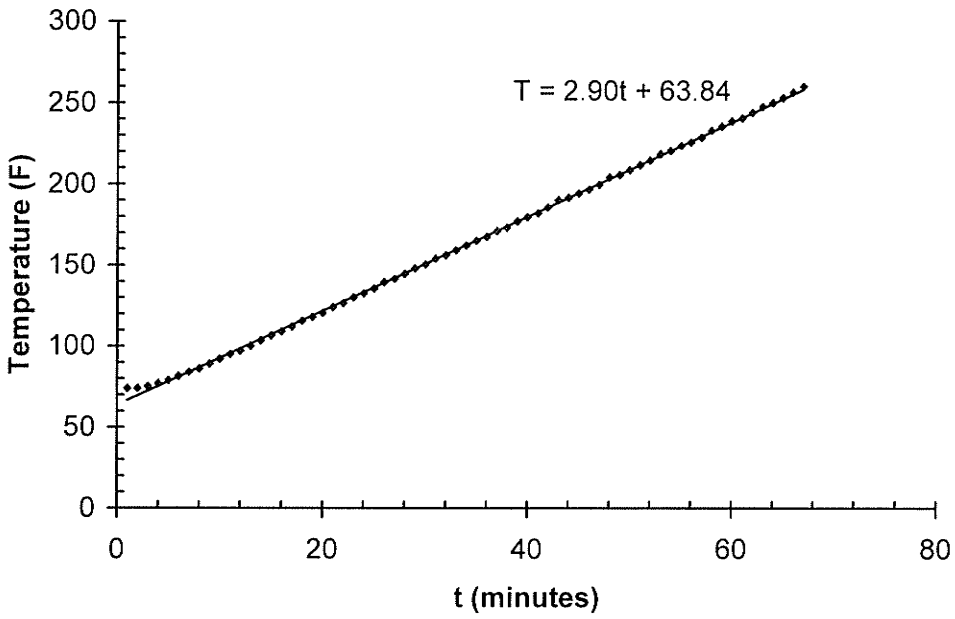

Figure 3.5: Measured tool temperature as a function of time for programmed ramp rate of 3 ^{0}F/min

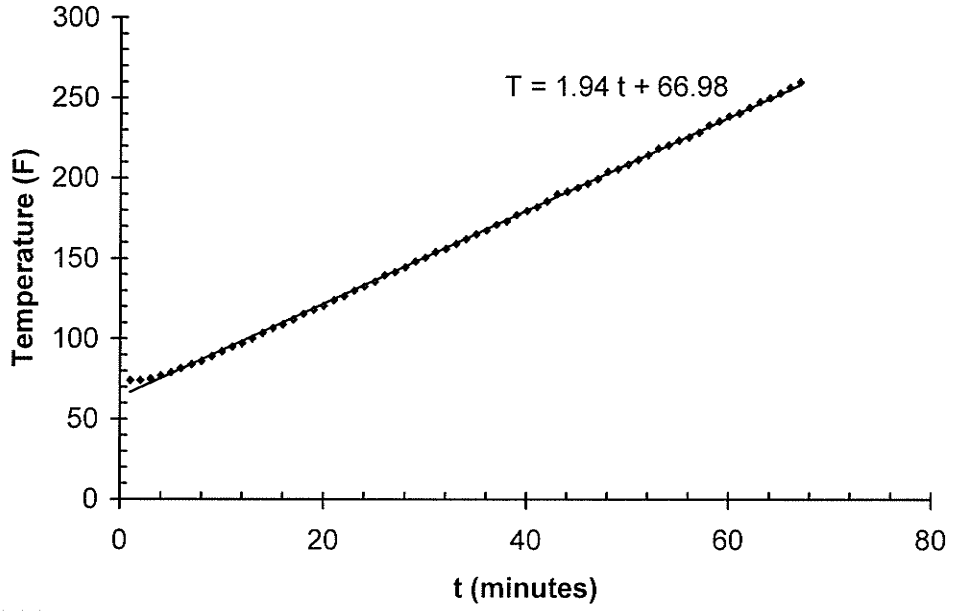

Figure 3.6: Measured tool temperature as a function of time for programmed ramp rate of 2 ^{0}F/min

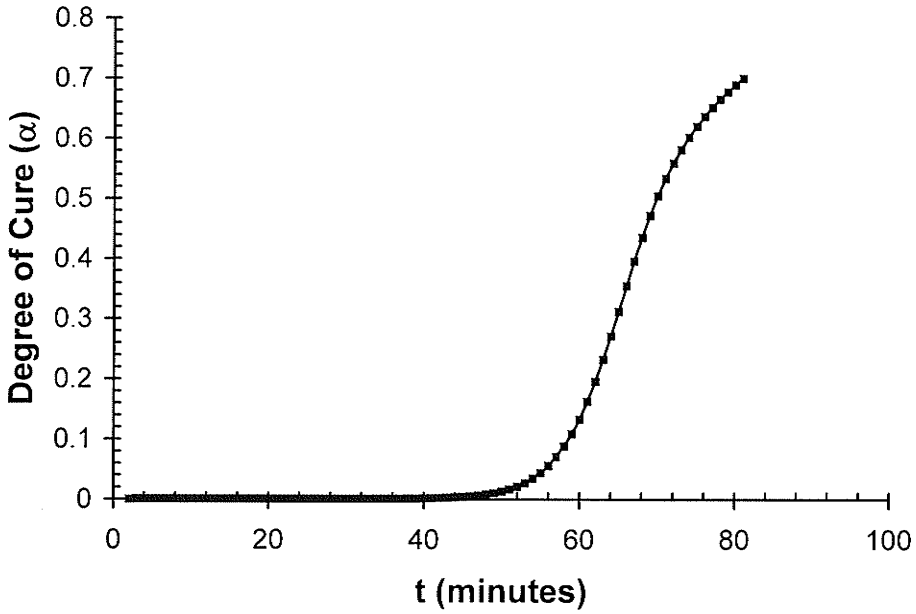

Figure 3.7: Experimentally determined degree of cure (α) as a function of time for ramp rate of 3 ^{0}F/min

The pull-out rate used in this study was about 1000 times more than the estimated tool-part sliding rate. The reason for this difference was to complete the experiment in a reasonable time so as to not allow the composite to cure significantly during the experiment. It was assumed that the frictional force was independent of the pull-out rate.

A 'National Instruments' data acquisition system (SCXI 1100 equipped with the 1131 module) was used to acquire the force and the displacement data during the test. A typical plot illustrating the variation of load with displacement is shown in Figure 3.8 for $\alpha = 0.2$ and a normal pressure 55 psi. The load increased to a maximum value, F_{static}, when the pre-preg specimen started to slide on the tool. Subsequently the load dropped rapidly to a constant value of $F_{dynamic}$ at which the pre-preg specimen slid and pulled away from the tool. Applying equation 3.1, the friction coefficients (μ_{static} and $\mu_{dynamic}$) were determined.

3.5 Design of Experiments

A design of experiments (DOE) methodology was used to delineate various factors affecting the tool-part interaction during autoclave processing. One parameter was varied at a time to analyze its significance on pull forces and the friction coefficients. The test plan shown in Table 3.2 was used in this thesis. Task 1 was to study the effect of the number of layers of composite materials and to see if there is any metal to metal interaction between the loading and the tool plates when a single layer of pre-preg was tested. The details of task 1 are explained below.

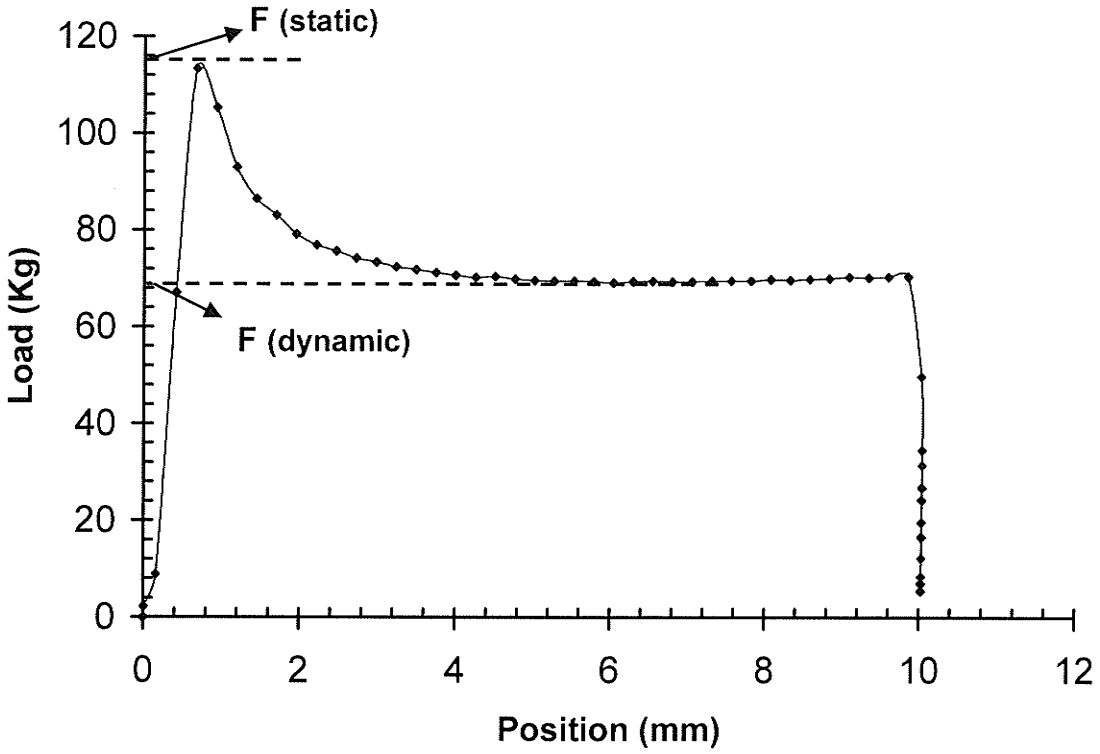

Figure 3.8: Typical plot illustrating variation of load with displacement

Table 3.2: Design of Experiments for the study of tool-part interaction

Design of Experiments		
Tasks #	**Experiment**	**Parameters**
1	Effect of test coupon thickness	Single Layer
		Two Layers
		Three Layers
		Four Layers
		Five Layers
2	Effect of Normal Load (Pressure)	193.2 Kg (35 psi)
		248.4 Kg (45 psi)
		304.6 Kg (55 psi)
3	Effect of Degree of Cure (α)	$\alpha = 0$
		$\alpha = 0.2$
		$\alpha = 0.4$
		$\alpha = 0.6$
		$\alpha = 1.0$
4	Effect of Temperature	Cure $T_1 = 260\ ^0F$
		Cure $T_1 = 287\ ^0F$
5	Effect of Ramp Rate ($3\ ^0F$/min and $2\ ^0F$/min)	$\alpha = 0$
		$\alpha = 0.2$
		$\alpha = 0.4$
		$\alpha = 0.6$
		$\alpha = 1.0$

3.5.1 Selection of number of layers of composite laminate for experiment (Task 1)

Preliminary experiments were done to determine the number of pre-preg layers to be used in the tool-part experiments. Ideally, one layer is preferred to avoid ply-ply slip and measure tool-part slip only. However, this raised a concern of possible metal to metal interaction, across the ply thickness, under the applied pressure. This could have potentially influenced the measured friction force and the friction coefficient. If there was any interaction, an increase in the number of layers would reduce the interaction and the measured slip load would decrease with an increase in number of layers, reaching a plateau.

The experimentally determined static frictional force (to be discussed in section 4.1) for a different number of layers of composite is tabulated in Table 3.3. The magnitude of friction forces for a different number of layers did not decrease with more layers. Hence, it was concluded that there was no metal to metal interaction in the case of the single layer. Hence, a single layer was used in all experiments. However, results summarized in Table 3.3 show that the magnitude of the pull force increased by 5% to 10% with the addition of each layer. The increase in pull loads might be due to the (visually observed) stretching of layers in the overhanging region (illustrated in Figure 3.1) with the increase in number of layers. Stretching in the overhanging region for a single layer is considered to be minimal. Moreover, since this contribution is the same for all measurements, their effect on observed trends in coefficient of friction is believed to be negligible.

Table 3.3: Measured F_{static} for $\alpha = 0$

Number of Layers	F_{static} (Kg)
Single Layer	189.6
Two Layers	210.5
Three Layers	220.8
Four Layers	230.8
Five Layers	252.8

3.5.2 Details of Task 2 to Task 5

Based on results of task 1 a single layer was used in all experiments. Task 2 was to study the effect of a variation in normal pressure. Since 310.3 kPa (45 psi) is usually used in the aerospace industry to cure honey-comb panels, it was used in this study to simulate the autoclave environment. As explained in Chapter 1, during the initial portion of the cure cycle the pressure inside the vacuum bag is -14.7 psi, resulting in a differential pressure, acting on the laminate (45 + 14.7 i.e. 59.7 psi). At a pre-determined time, the vacuum bag is vented to atmosphere when the differential pressure is (45 - 14.7 i.e. 30.3 psi). Hence, to study any variation in friction coefficients with a small change in pressure (+/- 15 psi), friction coefficients were also measured at 35 psi and 55 psi. Task 3 was to vary the degree of cure. Experiments were done for an α increment of 0.2 in the range of 0 to 1 to establish the trend of friction coefficients as a function of degree of cure. To understand the variation of friction coefficients at a higher degree of cure in task 2, task 3 experiments were done by curing the composite at two different temperatures. Finally the effect of cure history was studied in task 4 by repeating the task 2 experiments at a different ramp rate. Hence, by using the DOE methodology, the effect of various experimental parameters during the autoclave cure cycle on the friction coefficients was studied systematically.

CHAPTER 4

RESULTS AND DISCUSSION

4.0 Introduction

A systematic experimentation involving a number of parameters was completed to develop a sound understanding of the tool-part interaction. Tool-part interaction was studied through measurement of the coefficient of friction (μ) at the interface and its variation with the experimental parameters. These results are presented and discussed in this chapter. Also an error analysis based on analytical and experimental methods, was used to compute the magnitude of uncertainty in the experimental results.

4.1 Static and Dynamic Friction Coefficients

As discussed in Chapter 3 the static and dynamic friction coefficients were measured by using a double shear experiment in a specially designed test setup. Design of Experiments methodology (Table 3.2) was applied to study the variation of μ with each experimental parameter, as explained in the following sub sections. As discussed in section 3.5.1, only a single layer of composite was used in all subsequent experiments. A typical plot of the frictional force with displacement has been shown in Figure 3.8 and discussed in section 3.4.

4.1.1 Effect of Pressure

The measured F_{static} increased linearly with Normal load (N) according to Amontons' law and Coulomb's law, as shown in Figure 4.1 for an uncured sample. As discussed in

section 3.5.2, the normal load of interest in autoclave processing is 193-303 Kg. In the initial experiments, this range was extended to understand the effect of the normal load, if any, on the frictional force. The slope of data in Figure 4.1 (i.e., the μ_{static}), decreased for Normal loads $\geq$ 248 Kg. A similar trend was observed for $F_{dynamic}$ and $\mu_{dynamic}$, as shown in Figure 4.2 for $\alpha = 0$

Previous studies on the frictional properties of polymers and magnetic disks have also observed such a reduction in friction coefficient with an increase in the normal load [36, 37] for high values of normal load. This has been attributed to elastic (Hertizian) and plastic deformation of asperities on the contacts surfaces. When these deformed asperities break at sufficient large normal loads, the frictional coefficients will increase again due to trapping of their debris at the interface [38]. At relatively lower normal loads, when the adhesive forces are comparable to the contact force due to a normal load, the friction coefficient increases with a decrease in normal load [36]. The influence of adhesion in frictional stress was clearly shown by Attard [39] in his studies involving measurement of dynamic friction stress using AFM (Atomic Force Microscope).

The tool plate used in this study was coated with many layers of a non-stick coating to prevent adhesion between the tool plate and the composite pre-preg. Moreover, the tool surface was clear without any residual resin sticking to it, after removal of the pre-preg from the tool plate. Hence, neither the adhesion between the tool and the prepreg nor the adhesive failure of the pre-preg (i.e. tool - pre-preg interface) is believed to be the reason for the change in the slope.

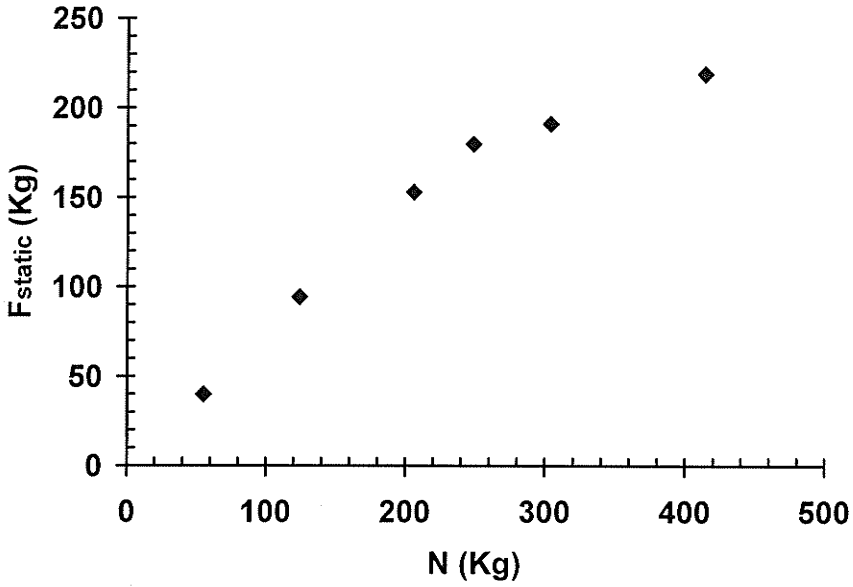

Figure 4.1: Variation of F_{static} with N for $\alpha = 0$

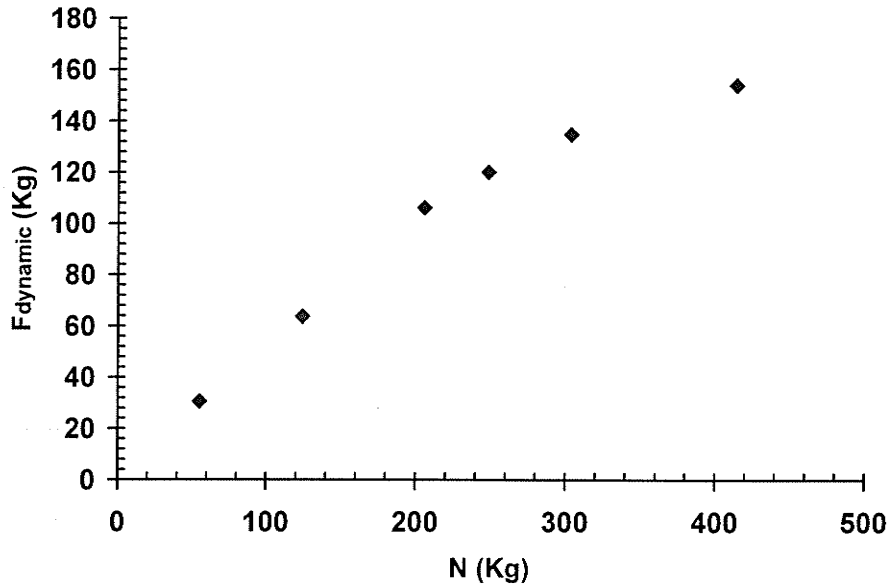

Figure 4.2: Variation of $F_{dynamic}$ with N for $\alpha = 0$

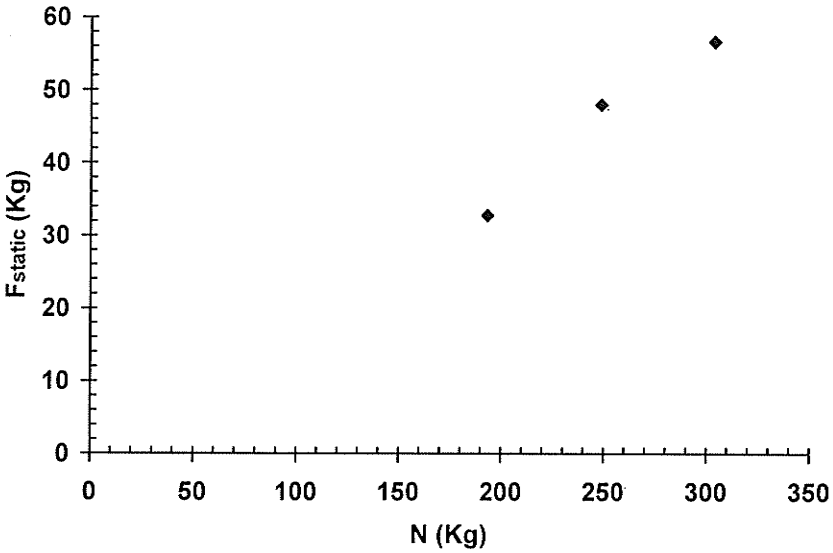

Figure 4.3: Variation of F_{static} with N for $\alpha = 0.2$

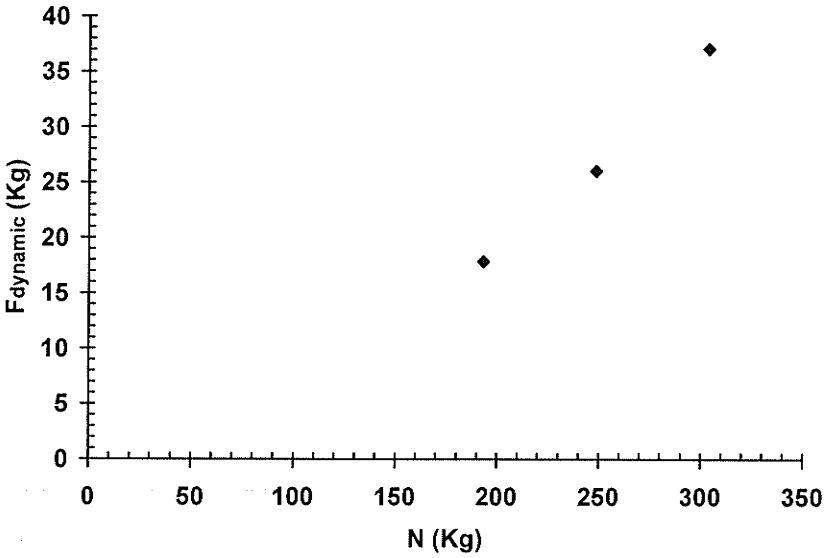

Figure 4.4: Variation of $F_{dynamic}$ with N for $\alpha = 0.2$

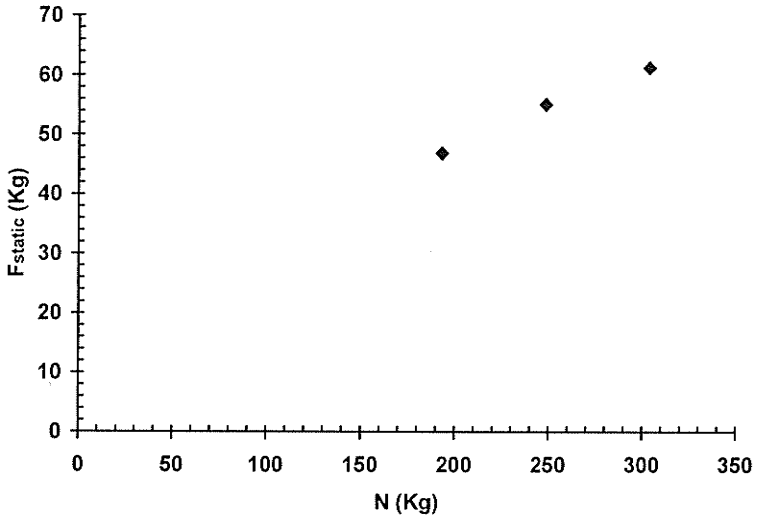

Figure 4.5: Variation of F_{static} with N for $\alpha = 0.4$

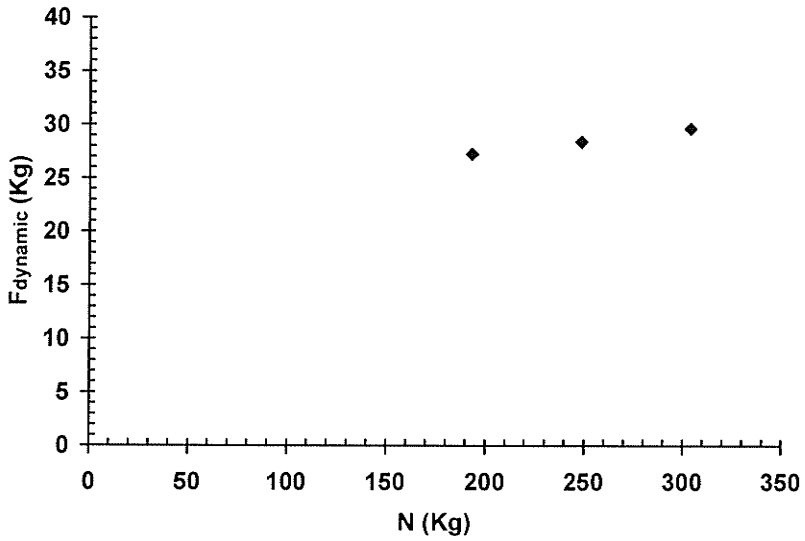

Figure 4.6: Variation of $F_{dynamic}$ with N for $\alpha = 0.4$

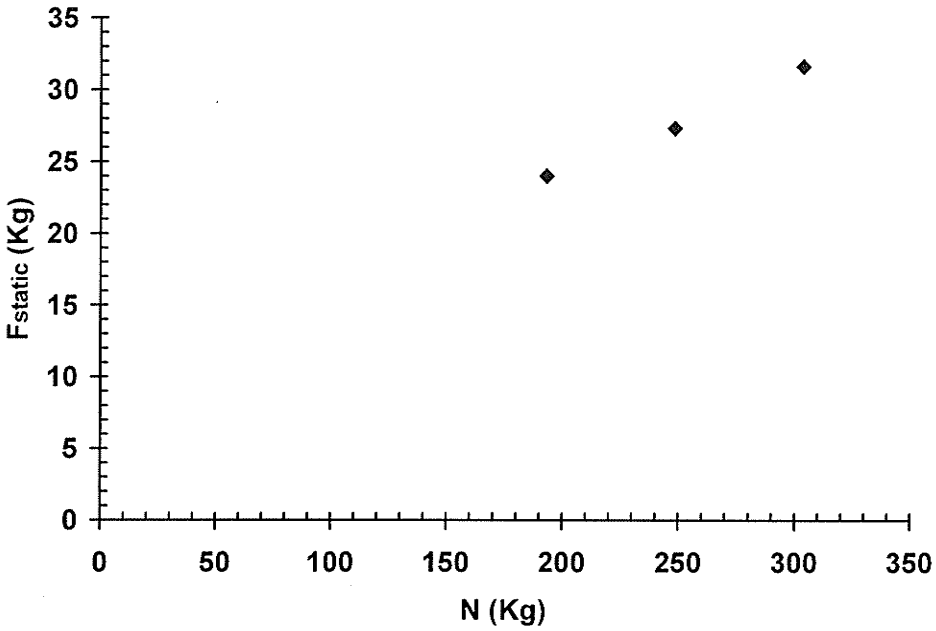

Figure 4.7: Variation of F_{static} with N for $\alpha = 0.6$

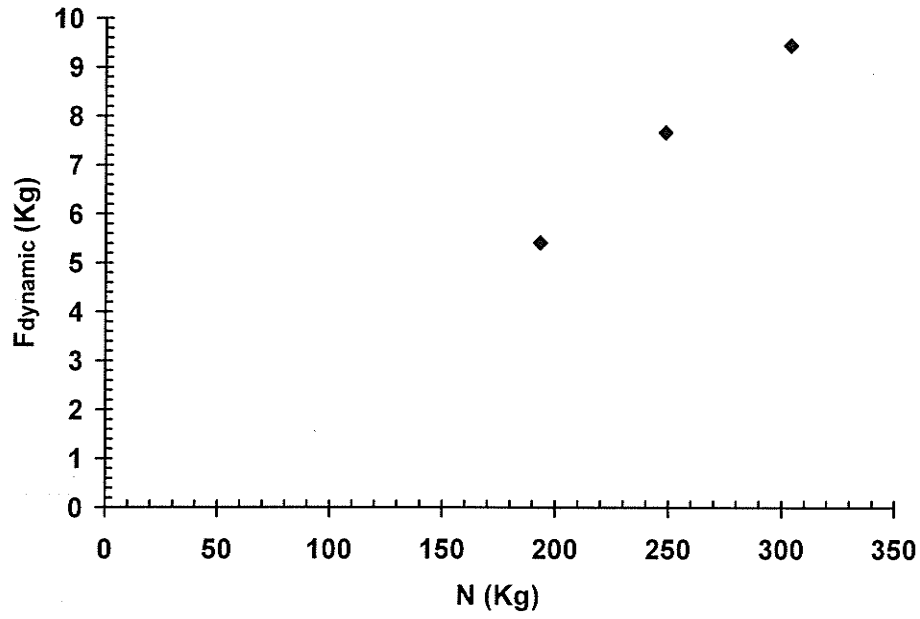

Figure 4.8: Variation of $F_{dynamic}$ with N for $\alpha = 0.6$

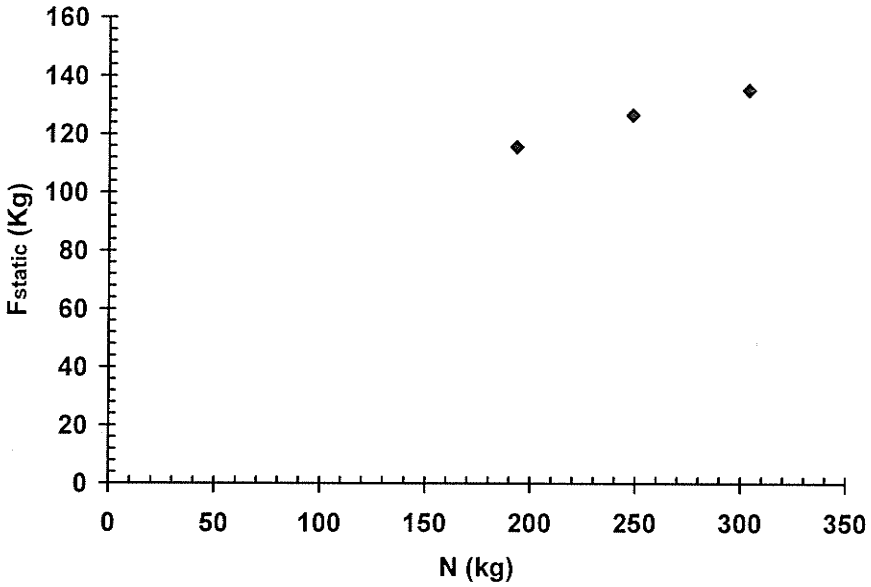

Figure 4.9: Variation of F_{static} with N for $\alpha = 1$

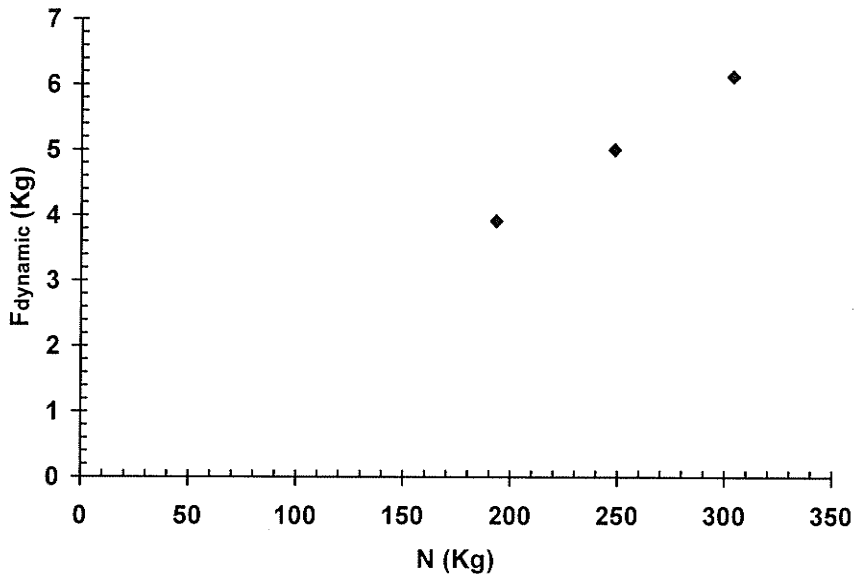

Figure 4.10: Variation of $F_{dynamic}$ with N for $\alpha = 1$

Since the resin in the pre-preg is uncured, it can easily flow under a normal load, decreasing the roughness of the pre-preg surface (similar to the plastic deformation of the asperities) caused by the crimp in the glass fibers. This is believed to have caused the reduction in the $\mu_{static\ and}\ \mu_{dynamic}$ beyond 248 kg.

For $\alpha \geq 0.2$, F_{static} and $F_{dynamic}$ increased linearly with the Normal load (N) according to Amontons' law and Coulomb's law, as shown in Figures 4.3 through 4.10. The μ_{static} and $\mu_{dynamic}$ calculated using these F_{static} and $F_{dynamic}$ are tabulated in Tables 4.1 through 4.5 for various α values. It can be observed that the μ values are independent of the Normal load in the usual range (193 - 303 Kg) of interest to autoclave processing, for all α values except $\alpha = 0$ and 1.0. Hence, the average of the μ_{static} and $\mu_{dynamic}$ values determined at the Normal load of 193 kg, 248 Kg and 303 Kg were tabulated in Table 4.6.

$\mu_{dynamic}$ was less then μ_{static}. This is a general trend observed in most of the published literature on friction.

4.1.2 Effect of Degree of Cure (α)

Experimentally determined μ_{static} values are plotted in Figure 4.11 for various degrees of cure (α) for an autoclave cure cycle with a programmed ramp rate of 3 ^{0}F/min. It decreased from a maximum value of 0.74 for $\alpha = 0$ to a value of 0.18 at $\alpha = 0.2$. Subsequently, it increased to a value of 0.22 for $\alpha = 0.4$ and again decreased to a value of 0.11 for $\alpha = 0.6$. It again increased to a value of 0.52 for a completely cured composite with $\alpha = 1$. Experimentally determined $\mu_{dynamic}$ are compared with μ_{static} in Table 4.2.

Table 4.1: Static friction at different normal loads for uncured composite ($\alpha = 0$)

P (kPa)	N (Kg)	μ_{static}	$\mu_{dynamic}$
68.9	55.2	0.72	0.55
155.1	124.2	0.76	0.52
257.2	205.9	0.74	0.52
310.3	248.4	0.72	0.48
380.2	303.6	0.63	0.44
517.1	414	0.53	0.37

Table 4.2: Static friction at different normal loads for $\alpha = 0.2$

P (kPa)	N (Kg)	μ_{static}	$\mu_{dynamic}$
241.3	193.2	0.17	0.09
310.3	248.4	0.19	0.10
379.2	303.6	0.19	0.12

Table 4.3: Static friction at different normal loads for $\alpha = 0.4$

P (kPa)	N (Kg)	μ_{static}	$\mu_{dynamic}$
241.3	193.2	0.24	0.14
310.3	248.4	0.22	0.11
379.2	303.6	0.20	0.10

Table 4.4: Static friction at different normal loads for $\alpha = 0.6$

P (kPa)	N (Kg)	μ_{static}	$\mu_{dynamic}$
241.3	193.2	0.12	0.03
310.3	248.4	0.11	0.03
379.2	303.6	0.10	0.03

Table 4.5: Static friction at different normal loads for $\alpha = 1.0$

P (kPa)	N (Kg)	μ_{static}	$\mu_{dynamic}$
241.3	193.2	0.60	0.02
310.3	248.4	0.51	0.02
379.2	303.6	0.45	0.02

Excepting α=0, the $\mu_{dynamic}$ were substantially lower than μ_{static} for all other α values, with $\mu_{dynamic}$ showing a similar trend as μ_{static} with increasing α. Flanagan [27] also observed a decrease in μ_{static} with increasing temperature during ramping up to cure temperature. However, he did not analyze the results in terms of the degree of cure (α).

4.1.2.1 Error Analysis

Errors in μ and α were determined to confirm the observed trend in μ given in Figure 4.11. This error analysis had two objectives. The first objective was to calculate the maximum percentage error in the friction coefficient. This was accomplished in the following two ways:

- Analytical determination of resolution in μ to make sure that it was much less than the experimental scatter. This was accomplished using the measurement of resolution of Force, Pressure and Area.
- Experimental determination of the error in μ by pursuing repeatability trials. By making sure that the experimental scatter in μ was less than the change in the mean value of μ with α, the trend in μ versus α was confirmed.

The second objective was to calculate the maximum percentage error in the predicted α and confirm that this error was much less than the experimentally recorded variation in α in order to confirm the observed trend in μ versus α. This was accomplished by comparing the α values determined using the Differential Scanning Calorimeter (DSC) curing experiment with the analytically determined α values from the cure-kinetics model used in predicting the 'α' values used in the Figure 4.11.

Table 4.6: Experimentally determined average friction coefficients (at 193.2 Kg, 248.4 Kg and 303.6 Kg normal load) for various α values

α	μ (static)	μ (dynamic)	Fracture of Surface
0	0.69 ± 0.02	0.480 ± 0.011	Clean (No Resin Stick)
0.2	0.18 ± 0.01	0.110 ± 0.003	Low Resin Sticking
0.4	0.22 ± 0.01	0.120 ± 0.003	High Resin Sticking
0.6	0.11 ± 0.00	0.030 ± 0.001	Low Resin Sticking
1	0.52 ± 0.01	0.020 ± 0.000	Clean (No Resin Stick)

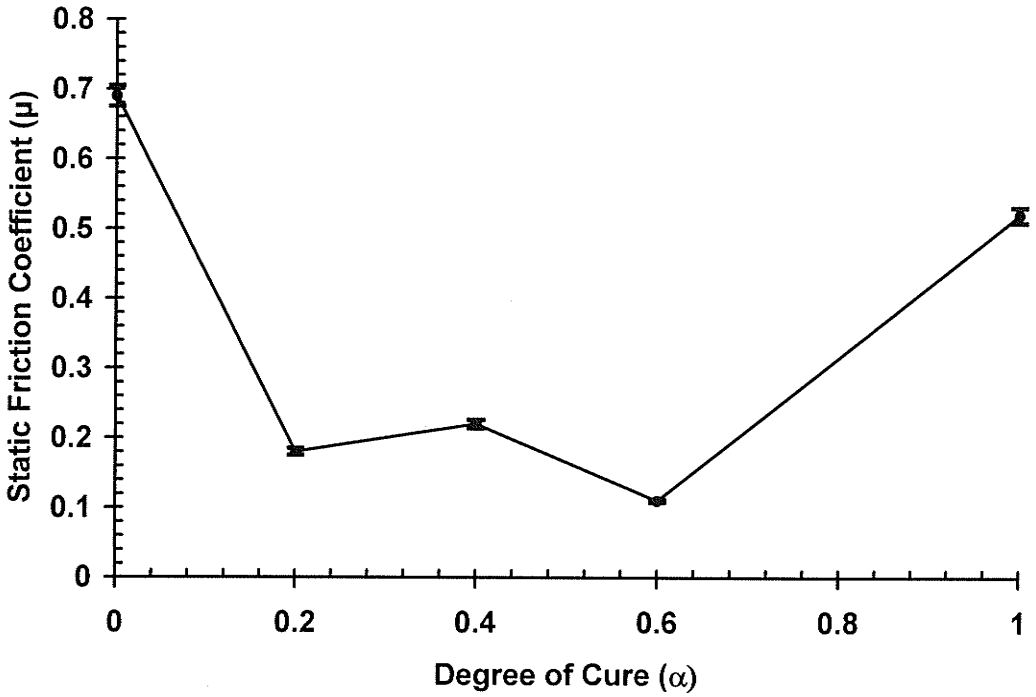

Figure 4.11: Variation of static friction coefficient (μ_{static}) with degree of cure (α)

4.1.2.1.1 Determination of error& scatter in μ.

Error occurs in prediction measurement due to precision of measurement and scatter (standard deviation) occurs in experimental values, due to repeatability issues (sample to sample difference). Precision error is normally < scatter.

A. Analytical determination of error in μ

This section provides an analytical determination of the error in μ based on the errors in the measured tangential force and normal force.

μ is defined as:

$$Friction Coefficient(\mu) = \frac{\text{Tangential Force (F)}}{\text{Normal Force (N)}} \tag{4.1}$$

where,

$$\text{Normal Force (N)} = \text{Normal Pressure (P)} \times \text{Load Cylinder Area (A)} \tag{4.2}$$

$$\therefore \mu = \frac{F}{P \times A} \tag{4.3}$$

also,

$$A = \frac{\pi \times D^2}{4} \tag{4.4}$$

The relative error (δ) is defined as the ratio of the absolute error (Δ) divided by the magnitude of the exact value. It gives an indication of how good a measurement is based on the magnitude of the parameter being measured. Also, the relative error of the quotient or product of a number of quantities is less than or equal to sum of their relative errors. Hence, using equation 4.4, the relative error in D is:

$$\delta D = \frac{\Delta D}{D} \tag{4.5}$$

Since Area (A) is proportional to the square of Diamater (D), using equation 4.4 and 4.5 the relative error in A is:

$$\delta A \leq \delta D + \delta D = 2\frac{\Delta D}{D} \tag{4.6}$$

Similarly, using equation 4.4 the relative error in μ is:

$$\delta \mu \leq \delta F + \delta P + \delta A \tag{4.7}$$

Combining equation 4.5 and 4.6,

$$\partial \mu \leq \frac{\Delta F}{F} + \frac{\Delta P}{P} + 2 \times \frac{\Delta D}{D} \tag{4.8}$$

For 310.3 kPa (45 psi), F, P and D are 110.2 Kg, 45 psi and 10 mm and the maximum absolute error i.e. resolution limit for F, P and D as 0.01 kG, 0.1 psi and 0.1 mm, respectively. Using these values the maximum percentage error in μ can be determined as

$$\delta \mu \leq (\frac{0.01}{110.20} + \frac{0.1}{45.0} + 2 \times \frac{0.1}{10.0}) \times 100\%$$

$$\delta \mu \leq 2.2\%$$

Similarly for P = 241.3 kPa (35 psi), $\delta \mu \leq 2.3\%$ and for P = 379.2 kPa (55 psi), $\delta \mu \leq 2.2\%$. Hence, for μ = 0.22 (peak position at α = 0.4), $\Delta \mu \leq 0.005$. Similarly, for μ = 0.18 (at α = 0.2), $\Delta \mu \leq 0.004$. Since the analytically determined maximum absolute error in μ is significantly smaller than the increase in its magnitude when α increased from 0.2 to 0.4, the observed trend in μ with α is real. Similarly the maximum absolute error in μ for other α values is also significantly smaller than corresponding μ values.

B. Experimental determination of scatter in μ

The repeatability tests were completed at α values of 0.2 and 0.4. Three sets of experiments were completed for each of the normal load values of 193.2 Kg (35 psi), 248.4 Kg (45 psi), and 303.6 Kg (55 psi) for both $\alpha = 0.2$ and $\alpha = 0.4$. The results are plotted in Figure 4.12 and Figure 4.13 and analyzed in Tables 4.7 and 4.8. X_m (the mean value) of μ_{static} was calculated at each of the pressure values and the deviation from the mean was determined for each repetition. Finally, the percentage scatter in μ_{static} was calculated as,

$$\text{Percentage scatter} = 100 * (X_m - X_i) / X_m \qquad (4.9)$$

The maximum observed scatter in measured F_{static} was about 3.2% which is of the same order as the error introduced by the resolution errors discussed in section 4.1.2.1.1 A. The scatter in μ_{static}, is $\pm$ 0.005 for $\alpha = 0.2$ and $\pm$ 0.006 for α =0.4. The scatter is less than the increase in μ_{static} (0.04) from α=0.2 to 0.4, which confirms that the observed trend in Figure 4.11 is real.

4.1.2.1.2 Experimental determination of error in degree of cure (α)

The degree of cure values used in Figure 4.11 and Table 4.6 were also tested for repeatability. The ramp rate of the composite specimen in contact with the tool plate was found to be 2.89 °F/min when the programmed rate was 3°F/min. Using this value and the cure kinetics parameters given in Table 3.1, the degree of cure was determined and used in the analysis. To confirm the accuracy of these predictions, the material was cured in a DSC using the same typical cure cycle including ramp, isothermal hold and cool down. The recorded heat flow curve (Figure 4.14) was used to compute the actual degree

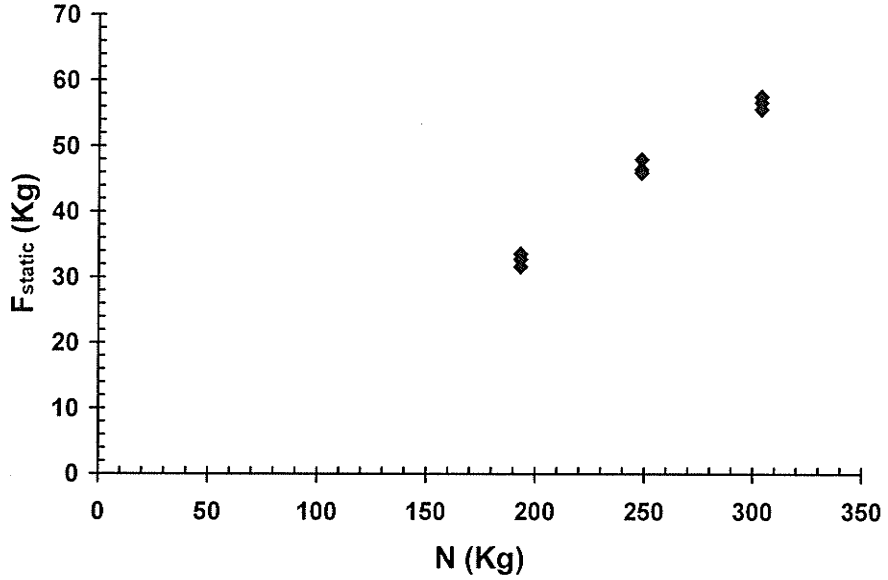

Figure 4.12: Repeatability experiments at $\alpha = 0.2$

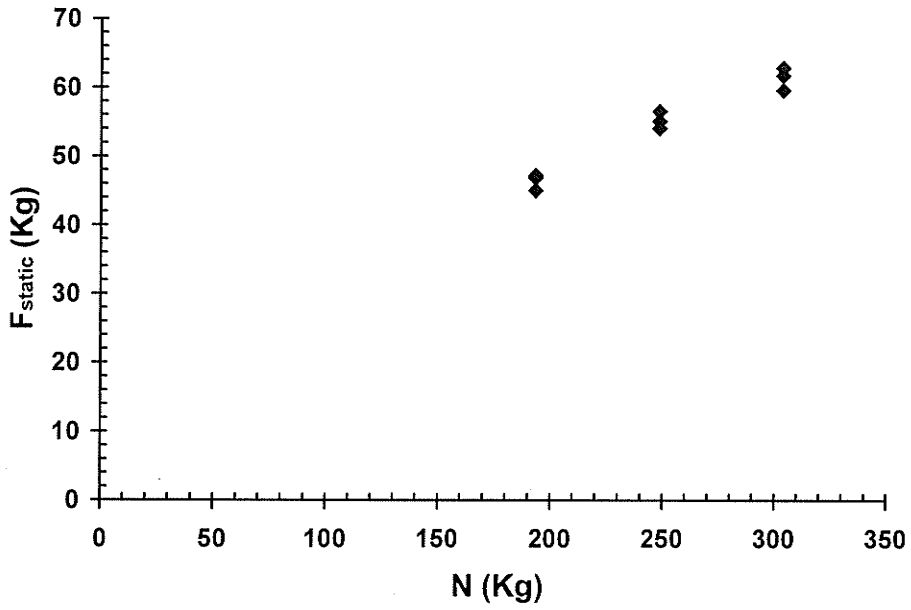

Figure 4.13: Repeatability experiments at $\alpha = 0.4$

Table 4.7: Repeatability experimental results for $\alpha = 0.2$

Run	Air Pressure (psi)	Air Pressure (N/m^2)	Cylinder Cross-sectional Area ($m^{2)}$	Face Area (m^2)	N (kg)	F_{static} (kg) (two surfaces)	F_{static} (kg) (one surface)	μ_{static}	X_m (mean value of μ_{static})	Deviation from mean value ($X_m - X_i$)	Scatter in μ_{static}
1a	35.0	241316.6	0.007854	0.0115	193.2	63.20	31.60	0.164	0.169	-0.005	**-3.2%**
1b						65.54	32.77	0.17		-0.001	**0.4%**
1c						67.10	33.55	0.174		0.004	**2.8%**
2a	45.0	310264.2			248.4	92.92	46.46	0.187	0.188	-0.001	**-0.7%**
2b						95.99	48.00	0.193		0.005	**2.6%**
2c						91.87	45.94	0.185		-0.003	**-1.8%**
3a	55.0	379211.8			303.6	111.21	55.61	0.183	0.186	-0.003	**-1.8%**
3b						113.32	56.66	0.187		0.000	**0.0%**
3c						115.16	57.58	0.19		0.003	**1.7%**

Table 4.8: Repeatability experimental results for $\alpha = 0.4$

Run	Air Pressure (psi)	Air Pressure (N/m^2)	Cylinder Cross-sectional Area (m^2)	Face Area (m^2)	N (kg)	F_{static} (kg) (two surfaces)	F_{static} (kg) (one surface)	μ_{static}	X_m (mean value of μ_{static})	Deviation from mean value ($X_m - X_i$)	Scatter in μ_{static}
1a	35.0	241316.6	0.007854	0.0115	193.2	93.74	46.87	0.243	0.24	0.003	**1.1%**
1b						90.02	45.01	0.233		-0.007	**2.9%**
1c						94.41	47.21	0.244		0.004	**1.8%**
2a	45.0	310264.2			248.4	110.2	55.1	0.222	0.222	0.000	**0.3%**
2b						108.1	54.05	0.218		-0.004	**2.2%**
2c						113.12	56.56	0.228		0.005	**2.4%**
3a	55.0	379211.8			303.6	123.5	61.75	0.203	0.202	0.001	**0.5%**
3b						119.21	59.61	0.196		-0.006	**2.9%**
3c						125.79	62.9	0.207		0.005	**2.4%**

of cure as a function of the process time for the applied autoclave cure cycle. (See Appendix C.) The predicted degree of cure using the actual specimen ramp rate is compared in Figure 4.15 with the degree of cure determined using DSC for the same cure cycle. Two sets of experimental runs were done with the DSC and both results are plotted in Figures 4.15 and 4.16. The maximum difference in the predicted and experimentally determined α values was 0.02 for the α range of values of 0.2 to 0.6. The difference increases for α values beyond 0.7, which reflects the inability of cure kinetics model to predict high α values with accuracy. However, this is not a major concern since no testing was done for α between 0.6 and 1.0. Since the scatter in α was significantly smaller than the values used in plotting the results the trend observed in Figure 4.11 is confirmed to be real.

The surfaces of the tool plates were examined after testing to understand the observed trend in Figure 4.11. Results of this examination are tabulated in Table 4.6. The tool surfaces were clean without any sticking resin at $\alpha = 0$. However, a tool plate covered with sticking resin was observed for $\alpha = 0.2$ and for $\alpha = 0.4$, as shown in Figure 4.17. Beyond this α value, the tool plate area covered with sticking resin decreased and the tool plates were clean without any sticking resin for $\alpha = 1$. A clean tool surface indicates that debonding and sliding occurred at the tool-part interface. If the debonding occurs by fracture of the part at a location away from the interface, then the tool surface will be completely covered with sticking resin. A partially covered tool surface, as observed in this study, indicates a fracture path that had straddled between the tool-part interface and

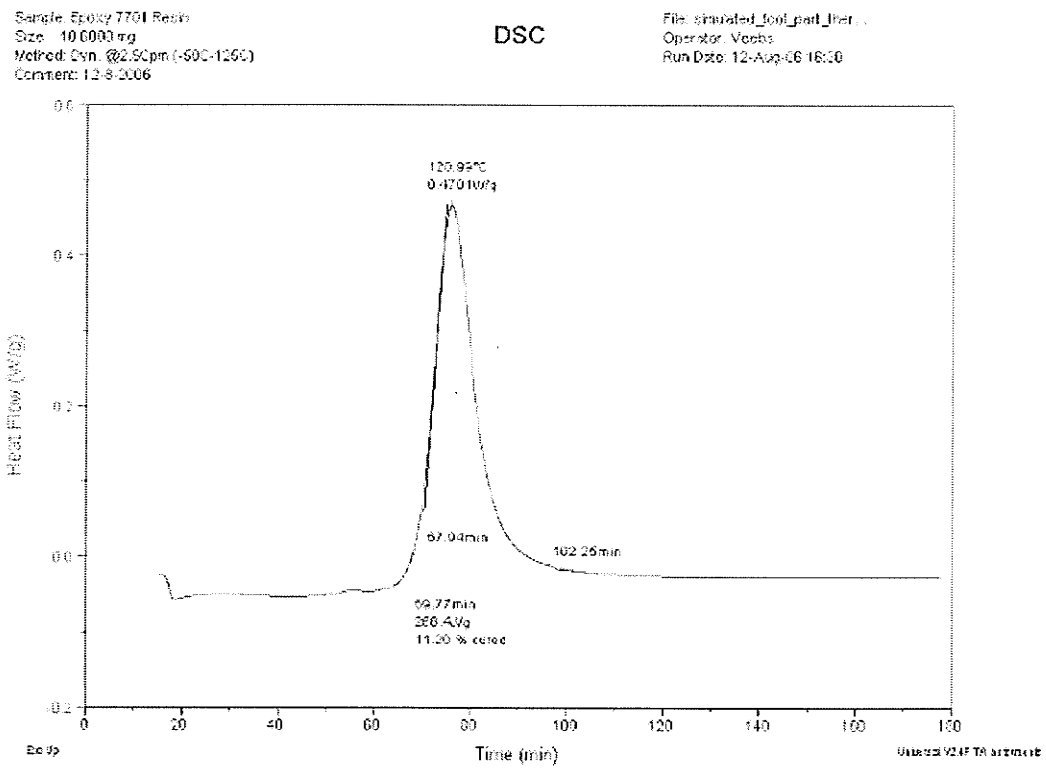

Figure 4.14: Heat Flow measured during DSC ramp experiment at 2.9 ^{0}C/min

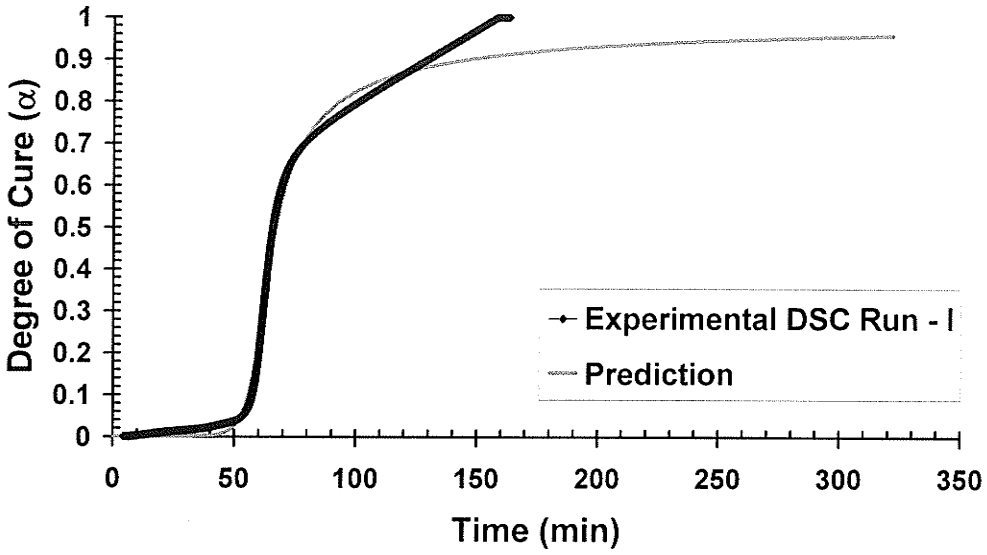

Figure 4.15: Comparison of simulated α with experimentally determined α at a ramp rate of 2.9 °C/min

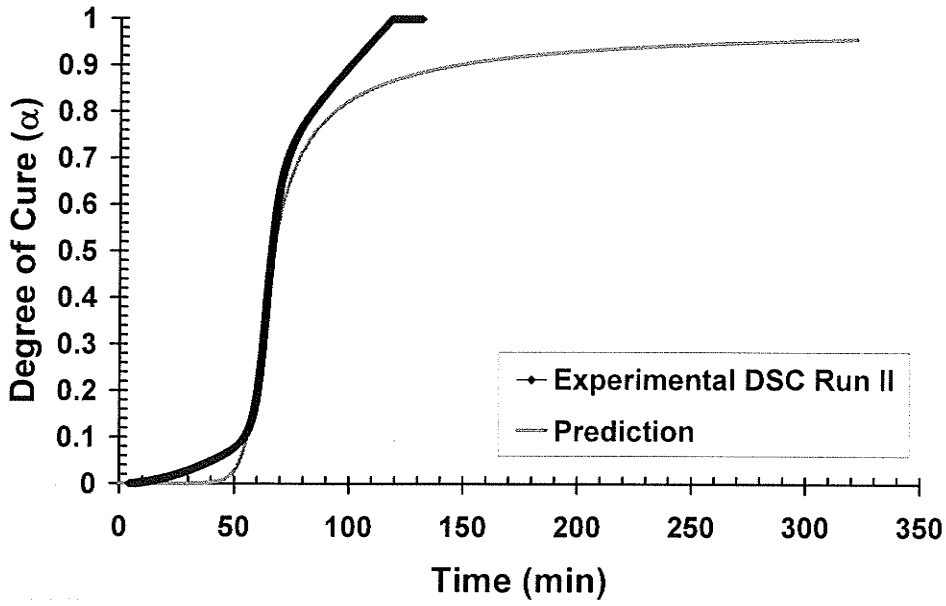

Figure 4.16: Comparison of simulated α with experimentally determined α at a ramp rate of 2.9 °C/min

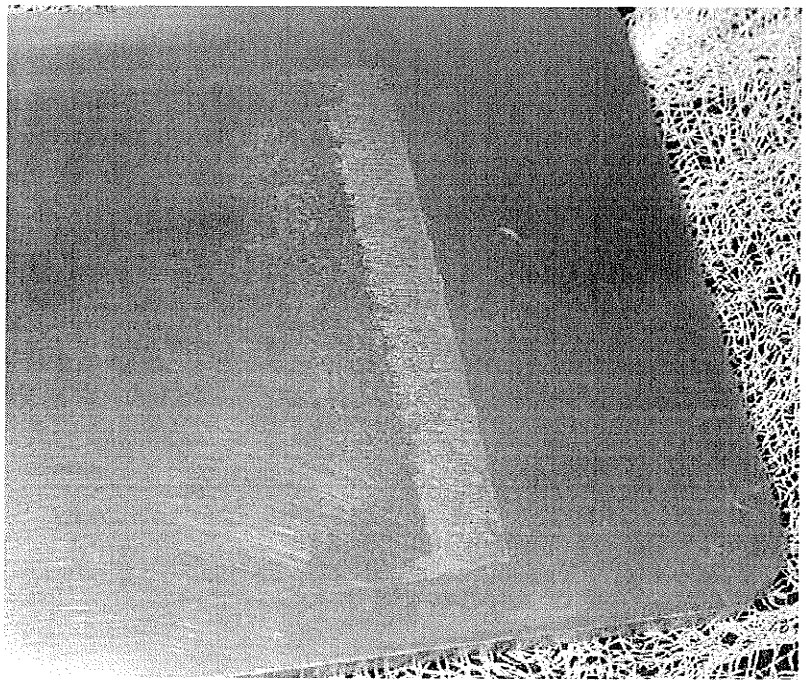

Figure 4.17: Photograph of the tool plate after testing at $\alpha = 0.4$, showing resin stuck to the tool plate

the part. The observed variation in the tool surface area, with sticking resin, with α indicates a changing tool-part interface, which is believed to be the reason for the observed trend in Figure 4.11.

A number of factors are believed to have contributed to this changing of the interface during the cure cycle, which can be understood using the schematic in Figure 4.18 - 4.22. Since the surfaces of the tool and the composite pre-preg are not smooth the contact between them at the interface, when the pre-preg is laid on the tool, may be as shown in Figure 4.18(a). Interactions between asperities on the two surfaces with possible mechanical interlocking are likely to be the cause of the high μ_{static} measured at α=0. Figure 4.18 (b) illustrates the tool and part surfaces after separation, a clean tool interface with no resin sticking indicates the fracture interface. During ramp-up to the cure temperature, the polymer matrix of the composite starts to flow due to a decrease in viscosity with increase in temperature and it may fill some crevices on the tool surface without bonding to the tool surface due to the non-stick coating on the tool surface as shown in Figure 4.19 (a). Simultaneously, the composite starts to cure. At α =0.2, the stiffness of the composite is low allowing it to easily deform, pull out of crevices, and slide over the asperities on the tool surface during testing. This may be aided by the reduction in the surface roughness of the pre-preg due to the flow of resin and easy shearing of resin, with low shear strength, that had filled the crevices on the tool surface. These trends, illustrated in Figure 4.19 (b), are believed to be the reasons for the reduction in μ_{static} when α increases to 0.2. With a further increase in α, the shear strength of the resin and stiffness of the composite will increase. Due to this, further

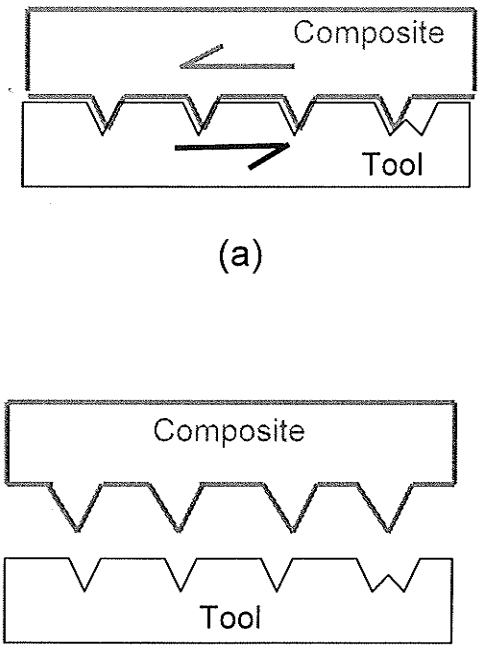

Figure 4.18: A schematic of (a) tool-part interaction during testing, and (b) tool part surfaces after testing at $\alpha = 0$

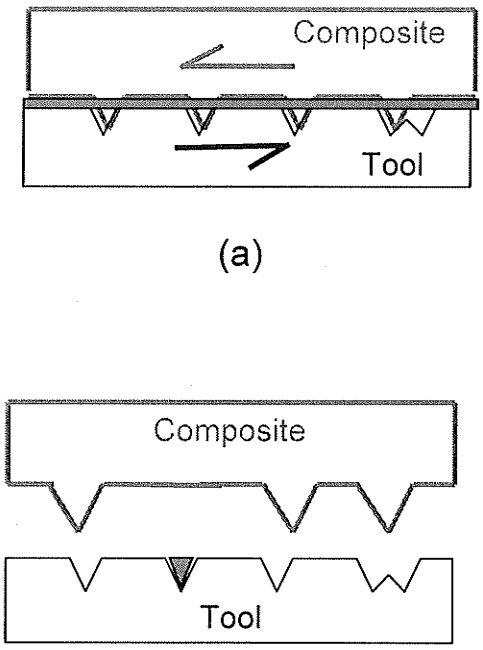

Figure 4.19: A schematic of (a) tool-part interaction during testing, and (b) tool part surfaces after testing at $\alpha = 0.2$

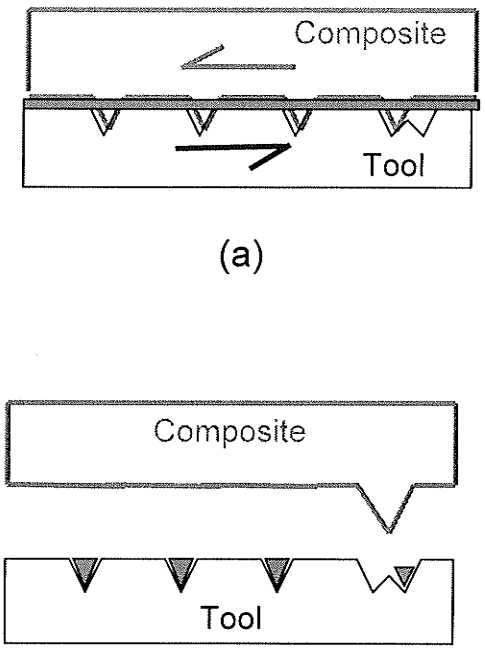

Figure 4.20: A schematic of (a) tool-part interaction during testing, and (b) tool part surfaces after testing at $\alpha = 0.4$

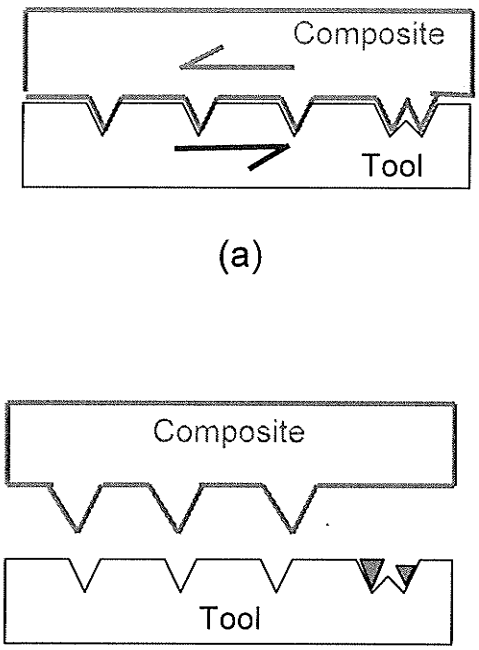

Figure 4.21: A schematic of (a) tool-part interaction during testing, and (b) tool part surfaces after testing at $\alpha = 0.6$

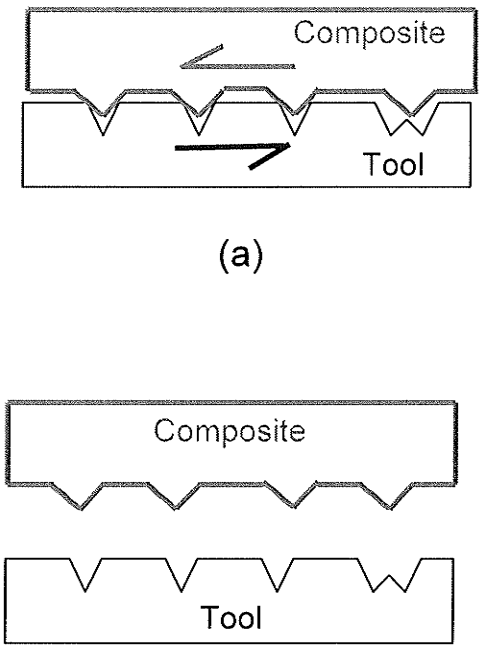

Figure 4.22: A schematic of (a) tool-part interaction during testing, and (b) tool part surfaces after testing at $\alpha = 1.0$

deformation and sliding the pre-preg requires more force. Instead of pulling out, resin in the crevices will fracture increasingly during testing, resulting in more resin sticking to the tool. These, illustrated in Figure 4.20 (b), are believed to be the reasons for an increase in μ_{static} from α equal 0.2 to 0.4. The resin matrix gels at $\alpha = 0.4$. Hence, beyond this α, the stiffness and strength continue to increase with further curing. Simultaneously, the cure shrinkage of the composite and resin starts to increase, which is believed to cause the resin within the crevices to pull away from walls of the crevices reducing the mechanical interlocking. This is believed to off-set the effect of increasing resin strength resulting in fracture of the resin at lower pull forces. Therefore, the μ_{static} decreases from $\alpha = 0.4$ to 0.6 and the tool surface area with sticking resin decreases as illustrated in Figure 4.21(b). Additionally, the cure shrinkage in the resin and composite will be resisted by the tool resulting in residual stresses in the former. The magnitude of this stress will increase with α due to an increase in stiffness of the composite and the resin. This is believed to be the cause for the increase in μ_{static} from $\alpha = 0.6$ to 1.0. The magnitude for μ_{static} (as well as force) at $\alpha = 1$ is less than that at $\alpha = 0$, even though the fracture path at the instant of debonding is along the tool-part interface for both cases. The fracture path is illustrated by the observed clean tool surface with no sticking resin as illustrated in Figure 4.22(b). This difference is due to the difference in the source of resistance to sliding of the pre-preg on the tool surface. While mechanical interlocking of the surfaces due to surface roughness is the source of resistance at $\alpha = 0$, residual stresses in the composite and tool are the sources of resistance at $\alpha = 1$. The low $\mu_{dynamic}$ at $\alpha=1$, compared to the $\mu_{dynamic}$ at $\alpha=0$, suggests sliding surfaces should have been relatively smoother at $\alpha = 1$ offering relatively less resistance to sliding. Since the tool surface

cannot change during curing, the surface of the composite should have become relatively smoother owing to the flow of the resin. The monotonic decrease in $\mu_{dynamic}$ with increasing in α is attributed to changing interface caused by (a) a change in fracture path for reasons discussed in the previous paragraphs, and (b) a change in smoothness of the composite surface due to resin flow below $\alpha = 0.4$.

4.1.3 Effect of Temperature

In order to confirm the interpretation in the previous section, the test for $\alpha = 1.0$ was repeated. However, the sample was cured and tested at 287 °F after ramping at 3 °F/min to 287 °F, whereas the sample discussed in previous paragraphs was cured and tested at 260 °F. The pull force (F) is plotted in Figures 4.23 and 4.24 as a function of normal force (N) for both samples. The recorded F value was much lower for the sample cured and tested at 287 °F than that at 260 °F at the same N value. The determined μ_{static} at 45 psi pressure (N = 248 kg) was 0.02 for the test at 287 °F while that at 260 °F was 0.52. It is believed that the composite debonded from the tool during curing owing to the development of relatively high levels of residual stresses at 287 °F, resulting in easy sliding during testing. This is supported by the experimental observation tabulated in Table 4.9. The μ_{static} and $\mu_{dynamic}$ for the test at 287 °F were identical and equal to $\mu_{dynamic}$ at 260 °F. This hypothesis on the impact of the residual stress on the measured friction coefficients is corroborated further in the next section.

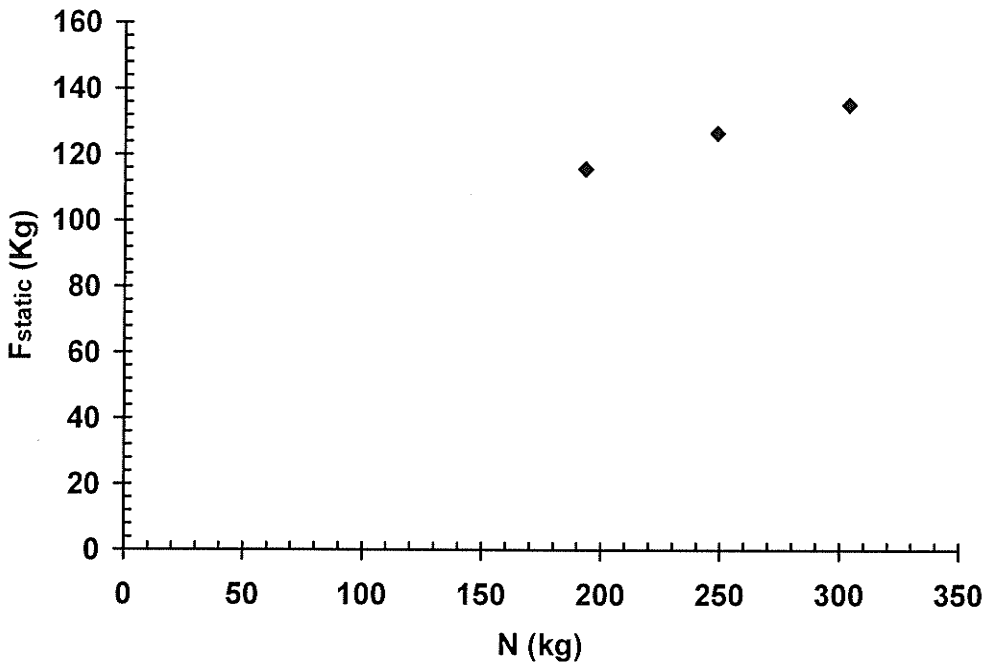

Figure 4.23: Variation of F_{static} with N for $\alpha = 1$ at 260 ^{0}F

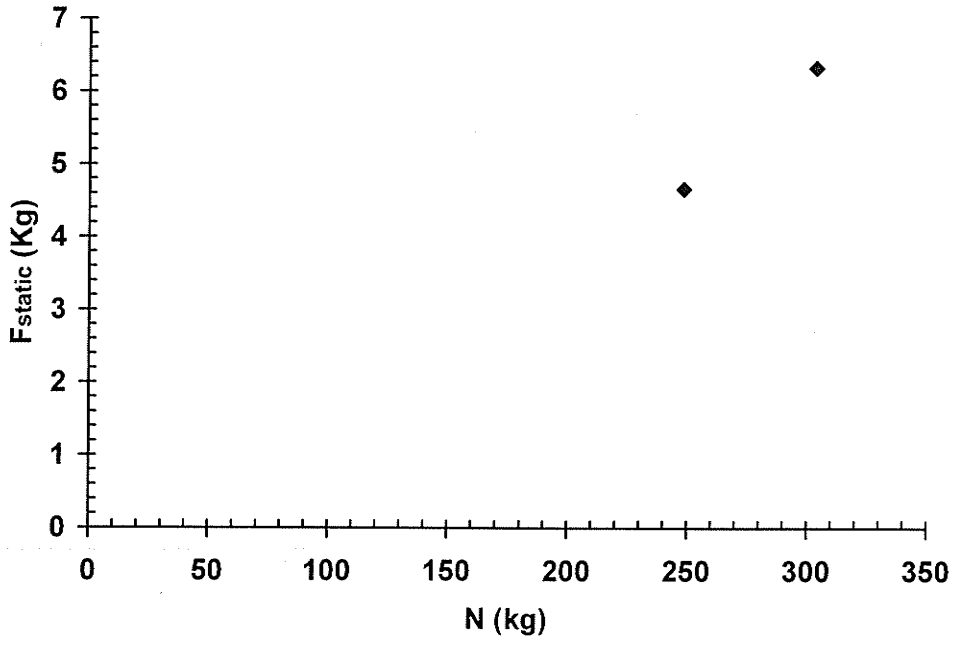

Figure 4.24: Variation of F_{static} with N for $\alpha = 1$ at 287 ^{0}F

Table 4.9: Variation of μ_{static} and $\mu_{dynamic}$ with cure temperature for $\alpha = 1$

T_{cure} (^{0}F)	N (kg)	μ_{static}	$\mu_{dynamic}$
260	193.2	0.60	0.02
	248.4	0.51	0.02
	303.6	0.45	0.02
287	248.4	0.02	0.02
	303.6	0.02	0.01

4.1.4 Effect of Ramp Rate on Tool-Part Interaction and Friction Coefficients

The results in the previous section indicate that resin flow, α and the path taken to achieve that α influence the friction coefficients by altering the interface. Since all these three factors can be affected by the ramp rate, an important parameter that defines the autoclave cure cycle, the latter was varied to understand how the autoclave cure cycle influenced the tool-part interaction.

The experimental results discussed in previous sections were obtained for a cure cycle with a programmed ramp rate of 3 °F/min. This experiment was repeated with another programmed ramp rate of 2 °F/min. The composite – tool assembly was ramped at 2 °F/min to the cure temperature of 260 °F, isothermally held at that temperature and cooled. A pull-out test was performed after reaching a desired α value. A new specimen was used for each α value. The time to reach a desired α value was determined using the plot in Figure 4.25 that was generated using the cure kinetics data given in Table 3.2 and the cure cycle ramp rate corresponding to the plot in Figure 3.5 for a controller ramp rate of 2 °F/min.

The experimentally determined friction coefficients are compared for the two ramp rates in Figure 4.26. While the friction coefficients were same for both rates for $\alpha \leq 0.4$, they diverged beyond α=0.4. The temperature and hence, the viscosity of the resin matrix, as well as the degree of cure of the composite at any process time will change with ramp rates. At 3 °F/min, the composite would have cured only to $\alpha = 0.2$ when the cure

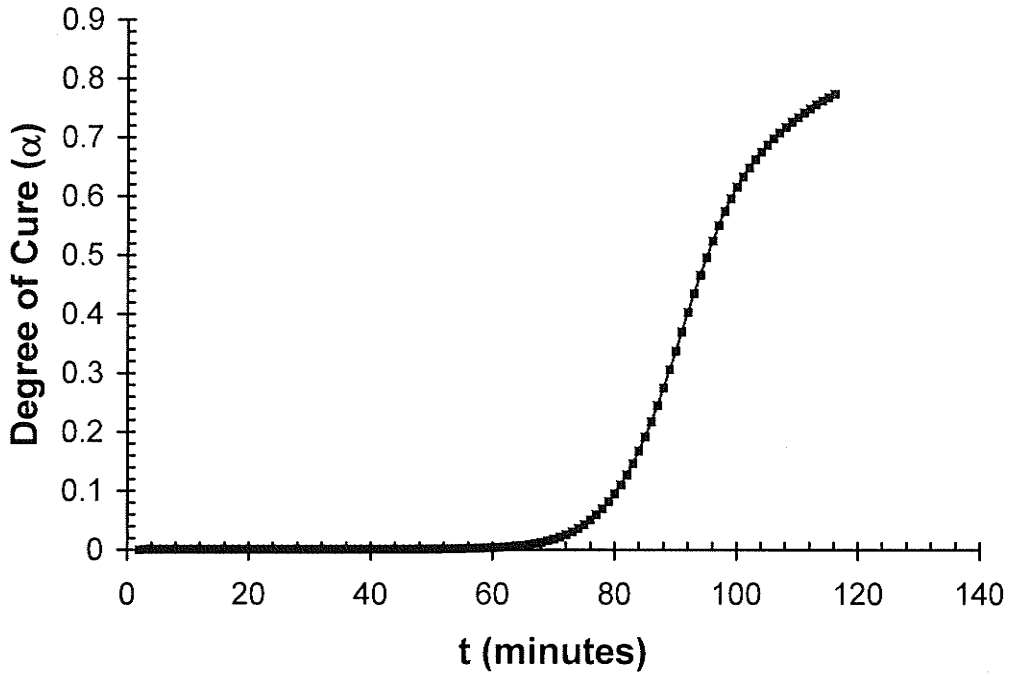

Figure 4.25: Experimentally determined degree of cure (α) as a function of time for ramp rate of 2 ^{0}F/min

temperature of 260 °F was reached. However, at 2 °F/min, the composite would have cured to α=0.2 well before the cure temperature of 260 °F is reached. At 2 °F/min, the composite would have taken 92 min to reach T_{cure} of 260 ^{0}F. Using the Figure 4.25, it can be concluded that the composite would have cured to 0.4. Hence, a slower ramp rate resulted in more curing during ramping than a faster ramp rate. Moreover, most of the curing (α = 0.2 to 1.0) occurred at a constant temperature of 260 ^{0}F in the case of 3 ^{0}F/min. In contrast, relatively less curing (α = 0.4 to 1.0) occurred at the constant temperature of 260 ^{0}F for 2 ^{0}F/min. This is the reason for the observed difference in Figure 4.26.

Below gelation (α_{gel} = 0.4) this difference in the cure rate would not matter since the change in interface is mainly due to resin flow. The minimum viscosity of the resin is expected to be low, at any given time before gelation, for high ramp rates. Since the composite chosen for this study is a high flow system with low minimum viscosity, the difference in viscosity and thus, the resin flow is envisaged to be minimal for the two ramp rates. This is believed to result in the same friction coefficients for both rates for $\alpha \leq 0.4$ In section 4.3, the increase in shear strength of the resin is suggested to be the cause for the increase in μ_{static} between α = 0.2 to 0.4. At 3 °F/min this increase occurred at a constant temperature of 260 °F while at 2 °F /min it occurred in a temperature range of 170 – 185 °F. Since strength normally decreases with an increase in temperature, one would expect the influence of this on the measured friction coefficients. Similar values for the friction coefficients suggest that this difference was not of sufficient magnitude to cause any impact.

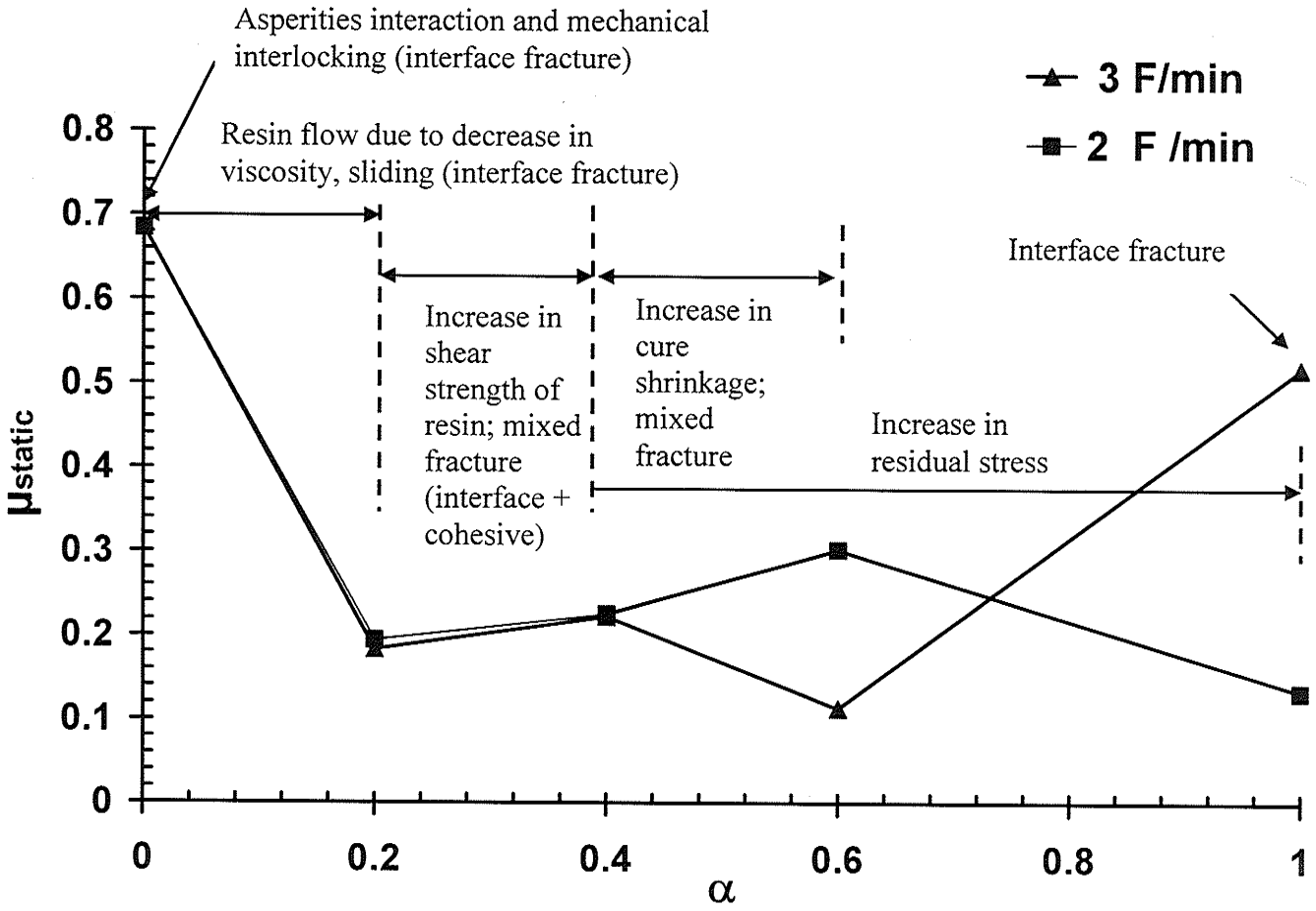

Figure 4.26: Variation of static friction coefficient with degree of cure for different ramp rates

As discussed in section 4.1 the factors that influence the interface and the friction coefficients are α, cure shrinkage strain, increase in strength and modulus of the resin and composite and residual stress. Since curing beyond $\alpha = 0.4$ occurs at a constant temperature of 260 °F, the only contributor to residual stress is the cure shrinkage strain when the composite and the tool is ramped at a rate of 3 °F/min. However, during ramping at 2 °F/min, the curing beyond $\alpha = 0.4$ occurs during ramping itself. Hence, thermal strains due to a differential expansion of the tool and the composite also contribute to the residual stress. Owing to this difference, the magnitude of the residual stress at any process time beyond gelation was higher for the lower ramp rate. This is believed to have led to increase in μ_{static} between $\alpha = 0.4 - 0.6$. Beyond $\alpha = 0.6$, the magnitude of the residual stress reached a critical value when the composite debonded from the tool, which is similar to the observation when the cure temperature was increased from 260 °F to 287°F. Therefore, during testing at α=1.0, the composite slid on the tool easily resulting in a lower μ_{static}. It is instructive to note that μ_{static} for 2 °F/min is equal to $\mu_{dynamic}$ for 3 °F/min, which confirms that the tool-part interface at $\alpha = 1.0$ is the same for both ramp rates. Hence, the difference in trend in μ_{static} beyond $\alpha = 0.4$ with the ramp rate is due to residual stress. This residual stress can be tensile or compressive and may have both tangential and normal components. Delineation of this is a complex task and it is beyond the scope of this study.

In summary, the tool-part interaction (quantification of μ) is a complex function of various mechanisms that come into play depending on the temperature and time of cure cycle (exemplified by α) in Figure 4.26.

4.2 Validation of Results in Tool-Part Interaction Study

Even though this validation was not done by the author of this thesis, the results of this thesis were used in this validation study. Hence, a brief summary of this validation study is presented here to highlight the practical relevance of this thesis.

The results of this study were used by Dr. X. Zeng and Dr. R. Jayaraman in an ABAQUS-based 3-D process model, developed by the Composite Materials and Structures Research Group at the University of Manitoba. In this model, the tool-part interaction was modeled using contact elements. The process-induced warpage of a fairing of a Boeing aircraft was predicted and validated experimentally. Figure 4.27 shows a picture of tool and composite used in autoclave manufacturing of strut fairing. Details of this study can be found in reference 20.

In Figure 4.28, the experimental and predicted part shape of a 2 - D cross section of the part after manufacturing is compared with the original shape of the uncured composite as laid on the tool. Due to symmetry only one half of the section is shown. While the maximum predicted warpage at the edge was 2.16 mm, the experimentally measured warpage was 2.57 mm. The maximum warpage measured at the edge of the part along the entire length of the part (6 feet) is compared with predictions in Figure 4.29. Very good correlation between the experimental and predicted values highlighted the practical relevance of the results of this thesis. In addition to the frictional interface, two other tool-part interface conditions were used in the predictions; a frictionless interface and a fully-bonded interface. It can be observed that the predictions using the frictional

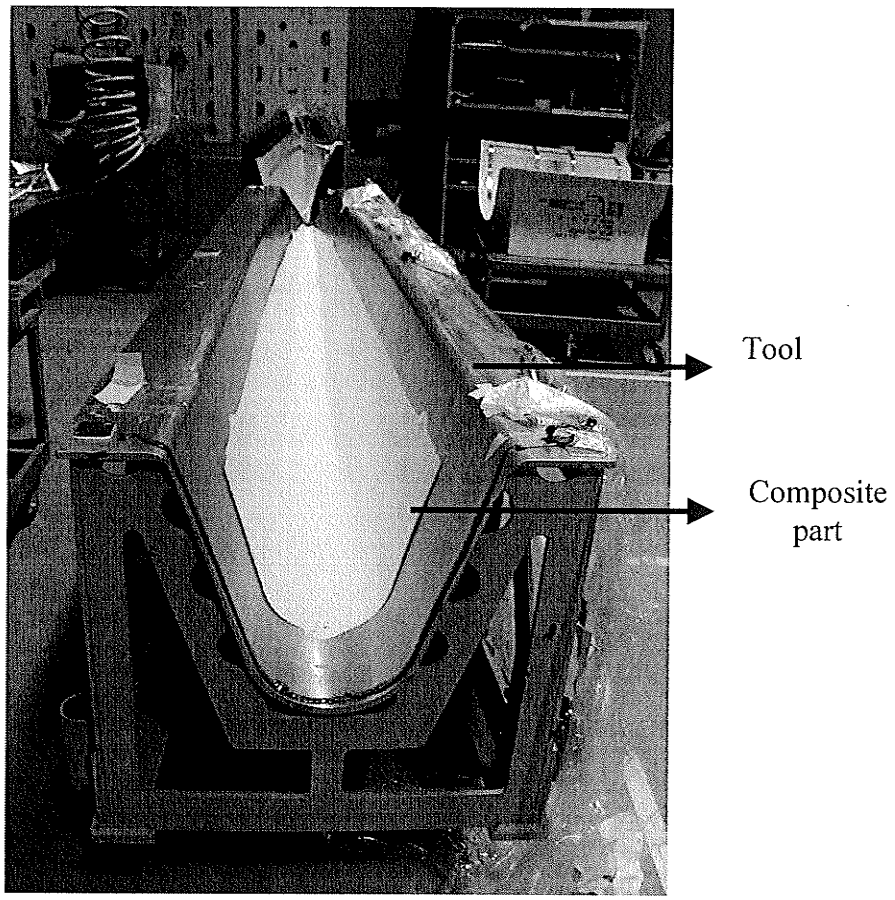

Figure 4.27: Composite pre-preg laid on the tool, shaped to manufacture strut fairing of Boeing 777 (Source: Boeing Canada Technology Ltd., Winnipeg)

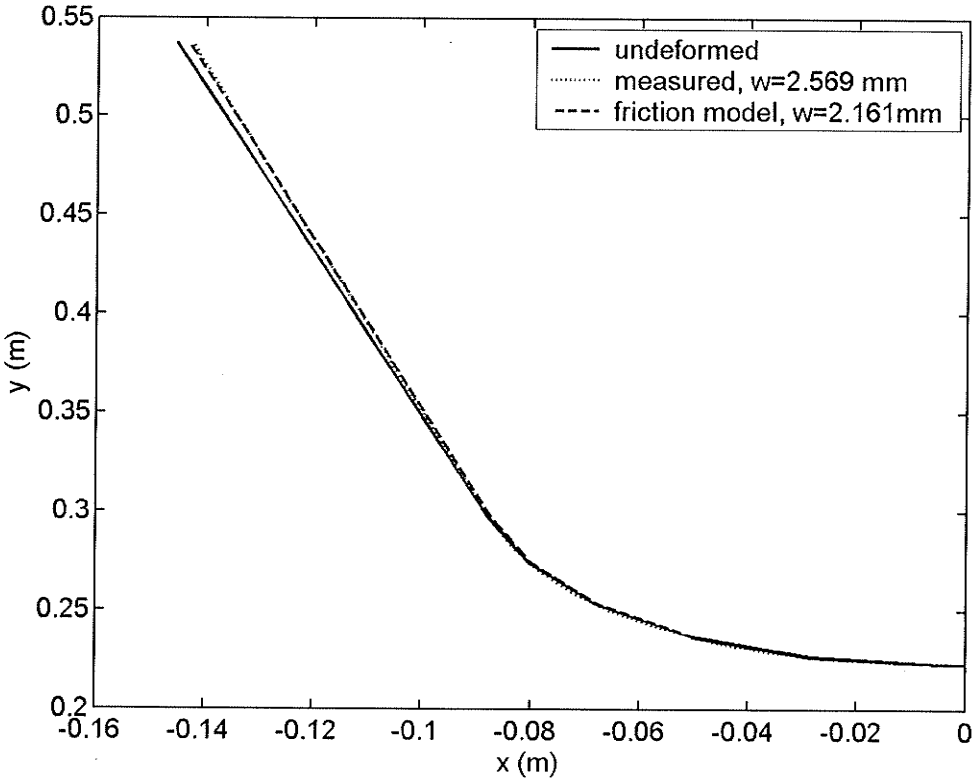

Figure 4.28: Comparison of experimental results and predicted part shape (one half of 2-D cross-section) after manufacturing with original shape of the uncured composite as laid on the tool. (Courtesy: R. Jayaraman)

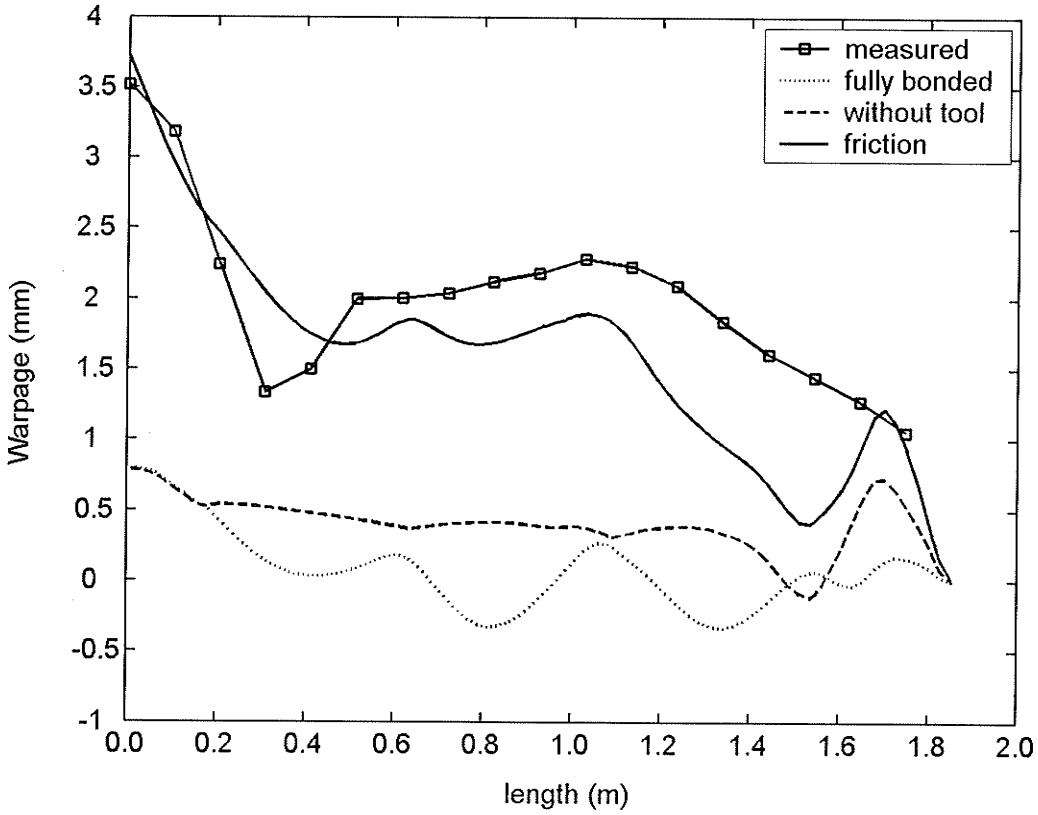

Figure 4.29: Comparison of measured and predicted maximum warpage as a function of the length of the part (Courtesy: R. Jayaraman)

interface and the experimental results of this study were realistic than the predictions using frictionless or fully bonded interface. This demonstrates the value of this thesis.

CHAPTER 5

CONCLUSIONS

In this study, tool-part interaction during autoclave processing of composite structures was experimentally studied by quantifying the friction between the tool and the composite. The static and dynamic friction coefficients were measured at the tool-part interface as a function of various influencing parameters such as thickness of the test coupon, pressure, degree of cure, cure temperature and ramp rate. The conclusions based on the current study and recommendations for future work are presented here.

5.1 Conclusions on Tool-Part Interaction Study

The current experimental study on tool-part interaction concluded the following:

- Both the static and dynamic frictional coefficients varied with the degree of cure (α) and ramp rate indicating that the frictional interaction between the tool and the part was a function of the autoclave cure cycle.
- The reasons for variation in static and dynamic friction coefficients were a continually changing tool-part interface, composite properties, and residual stress during the autoclave cure cycle.
- Application of the results of this study in an analytical model resulted in realistic predictions of the process-induced warpage of a composite structure of a commercial aircraft. This confirmed that frictional interaction between the tool and the part is a reality during autoclave processing of polymer composite structures despite the non-stick coating treatments given to the tools.

5.2 Recommendation for Future work

The following two recommendations were identified for future work:

5.2.1 Recommendation for future tool-part interaction work

This study was focused on studying the frictional interaction on tool-part interface as a function of autoclave cure cycle namely degree of cure and ramp rates (including temperature effect). The effect of misfit strain and aspect ratio of the part were not studied. The above two factors can also be taken as recommended future work.

5.2.2 Experimental results and discussion on ply–ply experiments and recommendation for future work

Study of ply-ply interaction in important for multi-layer laminate in which slippage may occur not only at the tool-part interface but also at the ply-ply interface. As discussed in chapter 2, Flanagan [27] used both the tool-part friction coefficient and ply-ply friction coefficient in a model to predict the warpage. Flanagan also measured both of these friction coefficients using a specially designed test rig. He concluded that tool-part friction coefficient is more significant factor in its contribution towards the warpage than ply-ply friction coefficient for multi-layer laminates.

In an attempt to study ply-ply friction in this thesis, the original test fixture was modified as shown in Figure 5.1. Laminate was prepared with two layers (of equal length) of composite pre-preg and was wrapped around the loading plate. However, in this case the outer layer was cut from the top (as shown in the schematic) to allow inter-ply slip with

the inner layer. In such a setup, slip can happen at either of the two interfaces, ply-ply or tool-part. Slip can occur between the outer layer and tool plate with the two layers behaving as a single unit. Alternatively, the slippage can occur between the two layers of composite with the outermost layer stuck to the tool plate and the inner layer stuck to the loading plate.

Experiments were done at three different pressures for zero degree of cure at room temperature. The measured load as a function of position is plotted in Figure 5.2 at 241.3 kPa (35 psi) for an uncured composite. As seen, instead of one peak there are two peaks in the plot, peak 1 at a higher load than peak 2. Similar plots for 310.3 kPa (45 psi) and 380.2 kPa (55 psi) for uncured composite are shown in Figure 5.3 and Figure 5.4. Also, the magnitude of load observed for all the three cases was found to be 10-20% higher than the magnitude of load observed in the same experiment for 2 layers with the top layer not cut from the top (tool-part friction only).

It is quite possible that the two peaks observed in Figure 5.3 and 5.4 correspond to tool-part interaction and ply-ply interaction. However the, assignment of these peaks to either of these two interactions requires additional study. Modifications in the experimental setup and test fixture are recommended for a future study of ply-ply slips only.

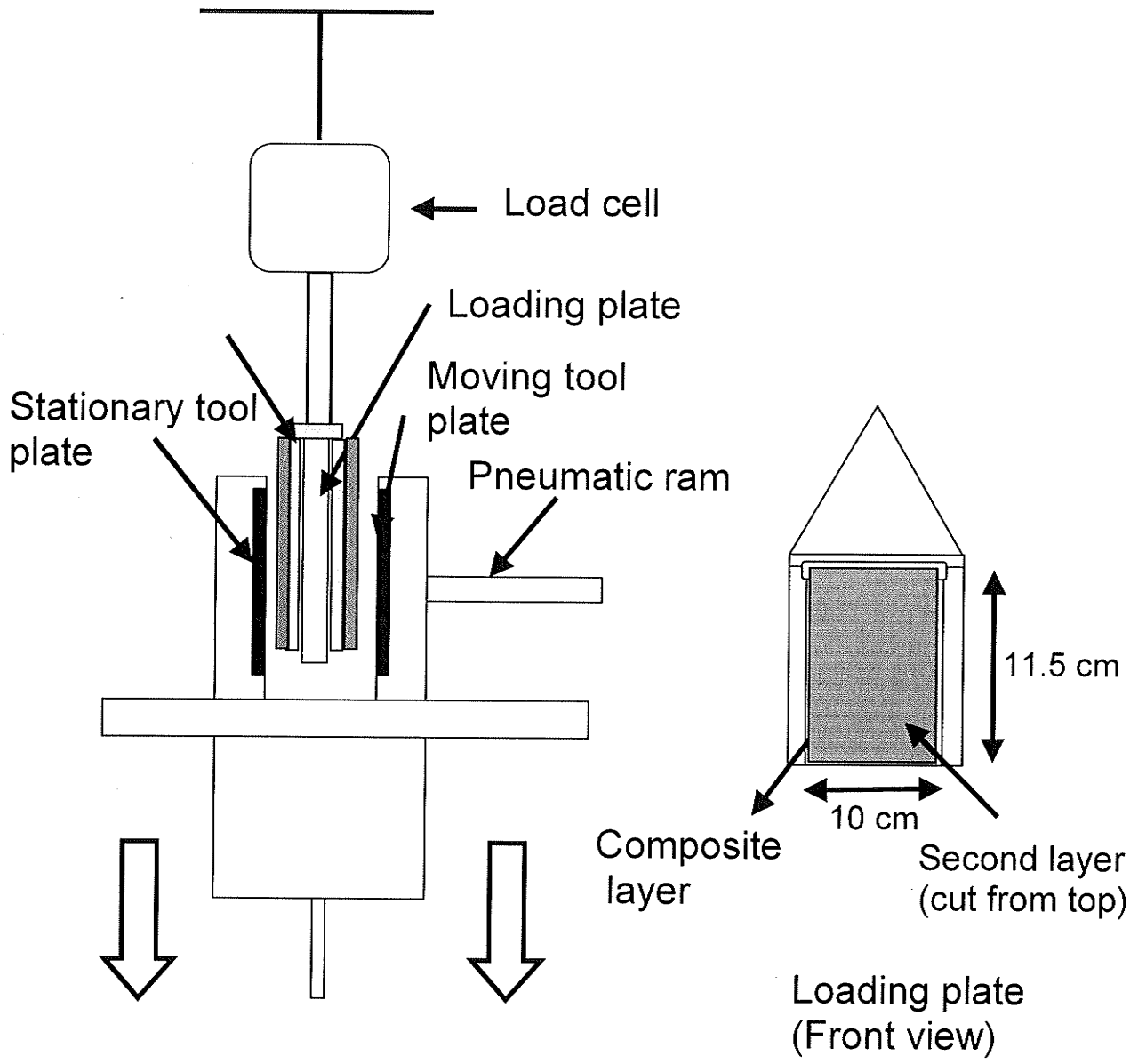

Figure 5.1: Schematic of the modified test fixture for study of ply-ply interaction

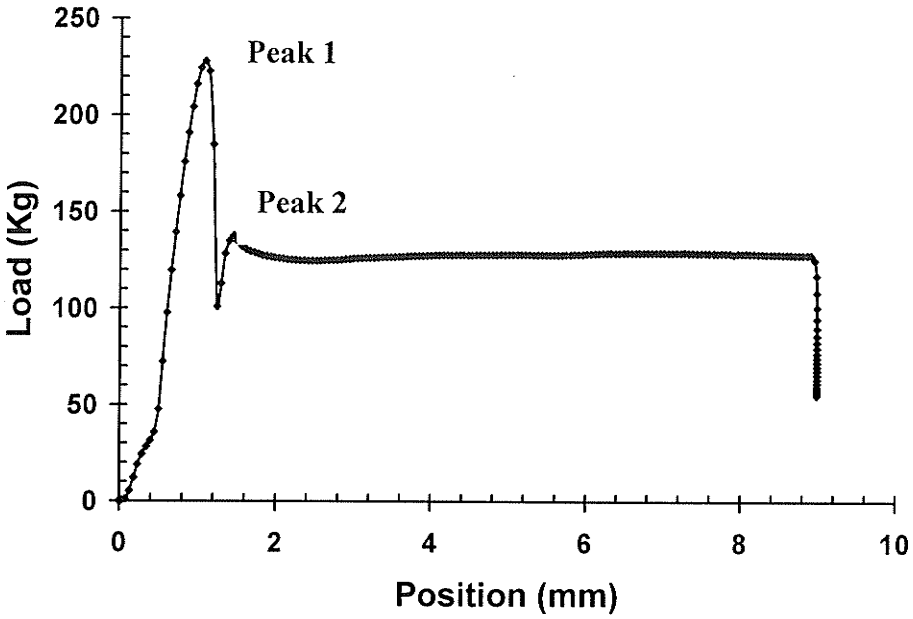

Figure 5.2: Ply-ply friction test results for α=0 and 241.3 kPa pressure

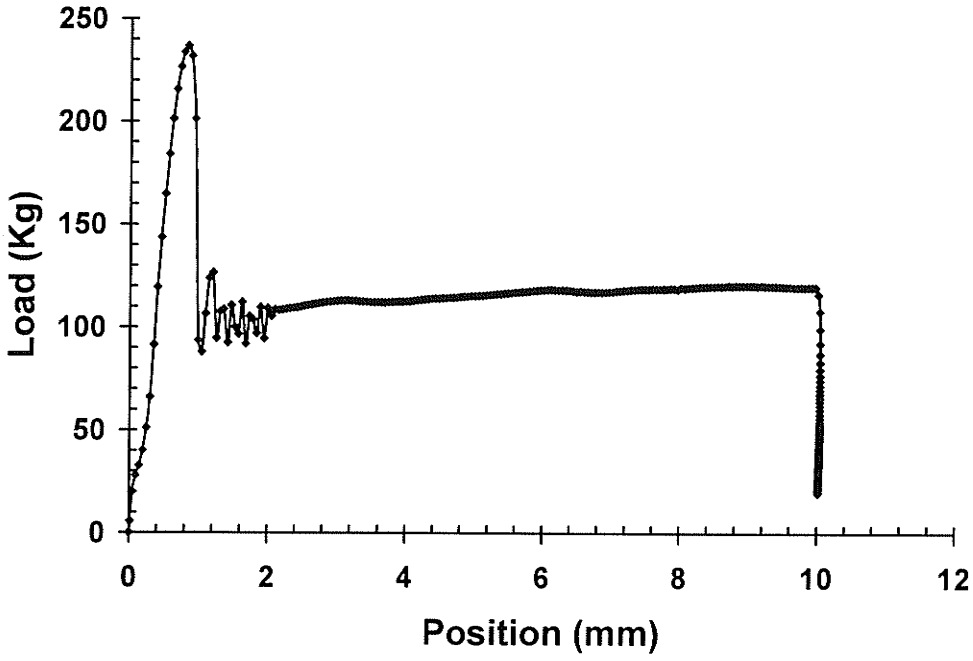

Figure 5.3: Ply-ply friction test results for α=0 and 310.3 kPa pressure

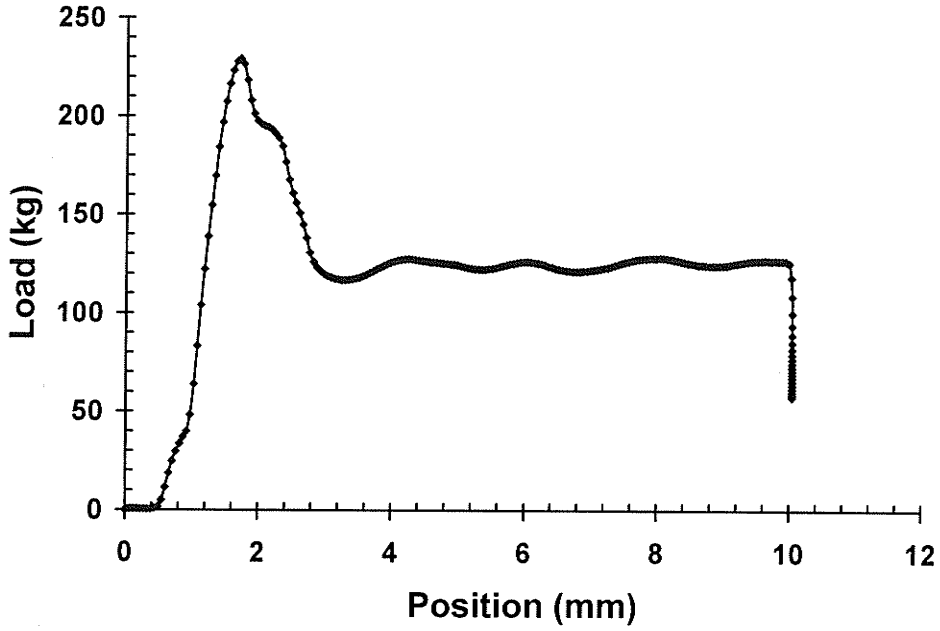

Figure 5.4: Ply-ply friction test results for α=0 and 380.2 kPa pressure

REFERENCES

1. Koteshwara M. P., "Parametric Study of Process-Induced Warpage In Composite Laminates", M.Sc. Thesis, University of Manitoba, August 2001
2. Koteshwara M. P. and J. Raghavan, "Parametric Study of Process-induced Deformation in Composite Laminates", Proceedings of 46th International SAMPE symposium and Exposition, Long Beach, CA, Vol. 46 II, (2001), pp. 2278-2292
3. Jain Lalit K, Mai Yiu-Wing, "Stress and deformation induced during Manufacturing. Part I", Journal of Composite Materials, Vol. 31, No.7, (1997), pp. 672-695
4. Jain Lalit K, Mai Yiu-Wing, "Stress and deformation induced during Manufacturing. Part II, A Study of spring in phenomenon", Journal of Composite Materials, Vol. 31, No.7, (1997), pp. 696-719
5. Sarrazin, H. B. Kim, S.H Ahn and G.S. Springer, "Effects of Processing Temperature and Lay-up on Spring Back", Journal of Composite Materials, Vol. 29, No. 10, (1995), pp. 1278-1294.
6. H.T Hahn and N.L. Pagano, "Curing Stresses in Composite Laminates", Journal of Composite Materials, Vol. 9, (1975), pp. 91-108
7. Alfred C Loos and George S Springer, "Curing of Epoxy Matrix Composites", Journal of Composite Materials, Vol. 17, (1983), pp. 135-169
8. T. A. Bogetti, "Process-Induced Stress and Deformation in Thick-Section Thermosetting Composites" , Technical Report CCM-89-32, Centre for Composite Materials, University of Delaware, Newark, Delaware, (1989)

9. White, S.R. and H.T. Hahn, "Process Modeling of Composite Materials: Residual Stress Development During Cure, part I. Model Formulation", Journal of Composite Materials, Vol. 26, No. 16, (1992), pp. 2402-2422

10. White, S.R. and H.T. Hahn, "Process Modeling of Composite Materials: Residual Stress Development During Cure, part II. Experimental Validation", Journal of Composite Materials, Vol. 26, No. 16, (1992), pp. 2423-2453

11. Pascal Hubert, "Aspects of Flow and Compaction of Laminated Composite Shapes During Cure", PhD thesis, University of British Columbia, (1996)

12. Michael Hudek, Matt Shewfelt, R.Mark Shead, Andrew Johnston, Nezih Mrad, Rick Cole, J. Raghavan, and Loren Hendrickson, "Examination of Heat Transfer in Autoclaves", Proceedings of International SAMPE symposium and exposition, Long Beach, CA, Vol. 46 II, (2001), pp. 2229-2242

13. M. Hojjati and S.V. Hoa, "Curing Simulation of Thick Thermosetting Composites", Composites Manufacturing, Vol. 5, (1994), pp 159-169.

14. J. Bailey, T. Bogetti, X. haung and W. Gillepse, "Cure Behavior of Thick-section Thermoset Composites", ANTEC, (1998), pp. 725-729.

15. Cann Michael T. and Adams Daniel O., "Effect of Part-Tool Interaction on Cure Distortion of Flat Composite Laminates", Proceedings of International SAMPE Symposium and Exhibition, Long Beach, CA, Vol. 46, (2001), pp. 2264-2274

16. Jose Daniel, D. Melo and Donald. W. Radford, "Modeling Manufacturing Distortions in Flat, Symmetric Composite Laminates", Proceedings of International SAMPE Technical Conference, Vol. 31, (1999), pp. 592-603

17. Pagliuso S., "Warpage, a Nightmare for Composite Parts Producers", In: Progress in Science and Engineering of Composites, Edited by Hayashi T, Kawata K, Umekawa S, proceedings of 4th International Conference of International Committee on Composite Materials (ICCM), Vol. 4, (1982), pp 1617-1623

18. Nelson R. H., Cairns D. S. "Prediction of Dimensional Changes in Composite Laminates During Cure", Proceedings of International SAMPE Symposium, Vol. 34, (1989), pp. 2397-2410

19. Ridgard C. "Accuracy and Distortion of Composite Parts and Tools: Causes and Solutions", Tooling for Composites published by SME (1993), pp. 91-113

20. Goran Fernlund and Anoush Poursartip, "The Effect of Tooling Material, Cure Cycle, and Tool Surface Finish on Spring-in of Autoclave Processed Cured Composite Parts", Proceedings of 12th International Conference of International Committee on Composite Materials (ICCM), Paris, France, paper 690, Vol. 12, (1999)

21. Twigg G, Poursartip A, Fernlund G. "An Experimental Method for Quantifying Tool-part Shear Interaction During Composites Processing", Composite Science and Technology, Vol. 63, No. 13, (2003), 1985-2002.

22. Twigg G, Poursartip A, Fernlund G. "Tool-Part Interaction in Composites Processing Part II: Numerical Modelling", Composites Part A, Vol. 35A, No. 1, (2003), pp. 135-141

23. Twigg G, Poursartip A, Fernlund G. "Tool-Part Interaction in Composites Processing Part I: Experimental Investigation and Analytical Modelling", Composites Part A, Vol. 35A, No.1, (2004), pp. 121-133

24. Johnston A, "An Integrated Model of the Development of Process-Induced Deformation in Autoclave Processing of Composite Structures. PhD Thesis, University of British Columbia, Vancouver, (1997)

25. Johnston A, Vaziri R, Poursartip A., "A Plane Stress Model for Process-Induced Deformation of Laminated Composite Structures", Journal of Composite Materials, Vol. 35, No. 16, (2001), pp. 1435 – 1469

26. Johnston A, Hubert P, Nelson K, Fernlund G and Poursartip A, "A Sensitivity Analysis of Modeling Predictions of the Warpage of a Composite Structure", proceedings of the 43rd International SAMPE Symposium, Vol. 43, No. 1, (1998), pp. 629-640

27. Flanagan Ronan, "The Dimensional Stability of Composite Laminates and Structures", Ph.D. Thesis, Queens University of Belfast, (1997)

28. J. Shi and R. Flanagan, "A Simple Spring-Damper-Slider Model for Laminate Slippage", Proceedings of the 10th International Conference on Composite Materials (ICCM), Vol. III, (1995), pp. 197– 204.

29. Bonin D, Characterization of the CYTEC BMS 8-79 7701 Epoxy Resin for the Undergraduate Thesis, Department of Mechanical and Manufacturing Engineering, University of Manitoba, (2004)

30. Cytec Engineering Materials, Tempe, Arizona., U.S.A. CYCOM 7701 Epoxy Resin Property Sheets, (1995) (Rev E) 013102.

31. X. Zeng, J. Raghavan, and V. Kaushik, "3-D Process Model For Autoclave Curing Of Large Composite Structures", Proceedings of SAMPE 2005 Long Beach Symposium, Vol. 50, (2005), pp. 413-426

32. V. Kaushik, Loren Hendrickson, X. Zeng and J. Raghavan, "Experimental Study of Tool-Part Interaction during Autoclave Processing of Thermoset Polymer Composite Structures for Aerospace Applications", To be submitted to Composites Part A.

33. V. Kaushik, Loren Hendrickson, X. Zeng and J. Raghavan, "An Experimental Investigation of Tool-Part Interaction During Autoclave Processing of Polymer Composite Structures", Proceedings of International Conference on Recent Advances in Composite Materials, Varanasi, India, (2004), pp. 101-106.

34. Zeng X., J. Raghavan, Loren P. Hendrickson, "3-D Process Model for Autoclave Processing of Large Composite Structures", To be submitted to Composites Part A.

35. Martin .C.J., J.C. Seferis, and M.A. Wilhem, " Frictional Resistance of Thermoset Pre-pregs and Its Influence on Honeycomb Composite Processing", Composites Part A, Vol. 27A, (1996), pp.943-951.

36. Etsion I, Amit M, "The Effect of Small Normal Loads on the Static Friction Coefficient for Very Smooth Surfaces", Proceedings of ASME Tribology Conference, Vol. 115, No. 3, (1993), pp. 406-410.

37. Pieter Samyn and Tony M Tuzolana, "Effect of Test Scale on the Friction Properties of Pure and Internal-Lubricated Cast Polyamides at Running-in", Polymer Testing, Vol. 26, (2007), pp. 660-675.

38. Bhushan B, Kulkarni, A.V, "Effect of Normal Loads on Microscale Friction Measurements", Thin Solid Films, Vol. 278, (1996), pp. 49-56.

39. Attard Phil, "Friction, Adhesion, and Deformation: Dynamic Measurements With Atomic Force Microscope", Journal of Adhesion Science and Technology, Vol. 16, No. 7, (2002), pp. 753-791.

40. Bowden F.P and Tabor D, "The Friction and Lubrication of Solids - Part 2", Oxford University Press, London, (1964)

41. Halling J, "Principles of Tribology", McMillian Press Ltd, London, (1978). Chapters 4, 10, 11 and 12

42. Currier A, "A Theory of Friction", International Journal of Solids and Structures, Vol. 20, (1984), pp. 637-640

43. Hutchings I.M, "Tribology: Friction and Wear of Engineering Materials", Edward Arnold, London, (1992), Chapters 2, 3 and 4.

APPENDIX A

A PRIMER ON FRICTION

The theory of friction is a part of the general area of Tribology, or the 'science of rubbing'. The following section is a discussion of the current thinking on physical causes of friction. The discussion has been taken from three major sources, Bowden and Tabor [40], Halling [41], Currier [42] and Hutchings [43]. Friction is effectively the resistance encountered by one body as it moves over another. Three basic laws apply;

Amontons' laws (first described by Leonardo De Vinci)

- friction is independent of the apparent contact area
- The friction force is proportional to the normal load as illustrated in Figure A.1

However, this law does not provide an estimate for the frictional force.

The threshold value when the sliding start was provided by Coulomb's approximation. Coulomb added a third law according to which

- The kinetic friction is independent of the speed of rubbing as illustrated in Figure A.2

Coulomb's friction defines friction coefficient (or coefficient of friction) as the ratio of the tangential reaction force of friction between the two bodies and the normal force pressing them together. The coefficient of friction is a dimensionless scalar value and

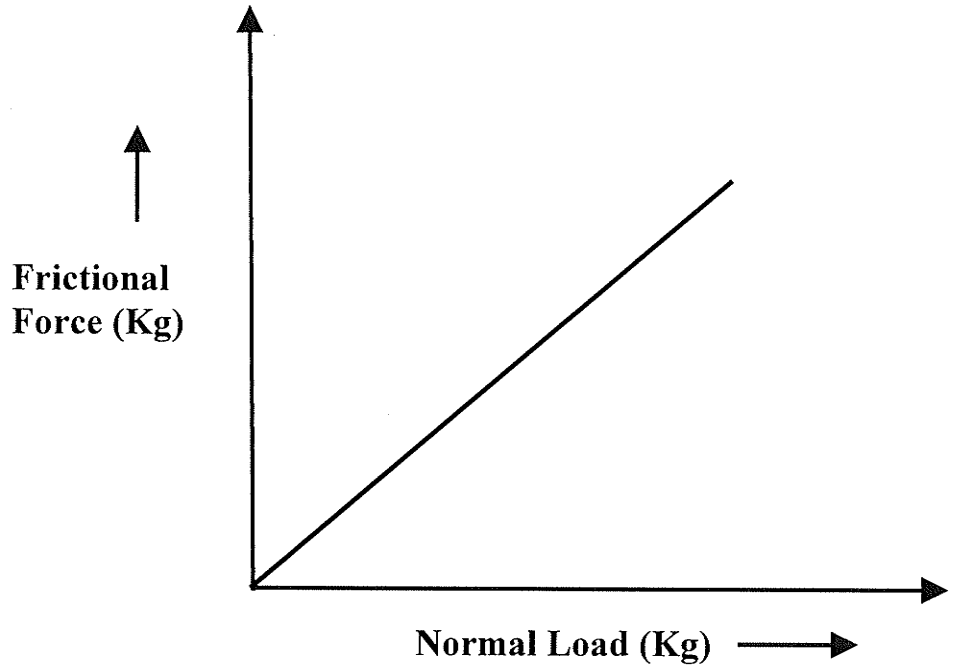

Figure A.1: An illustration of Amontons' law

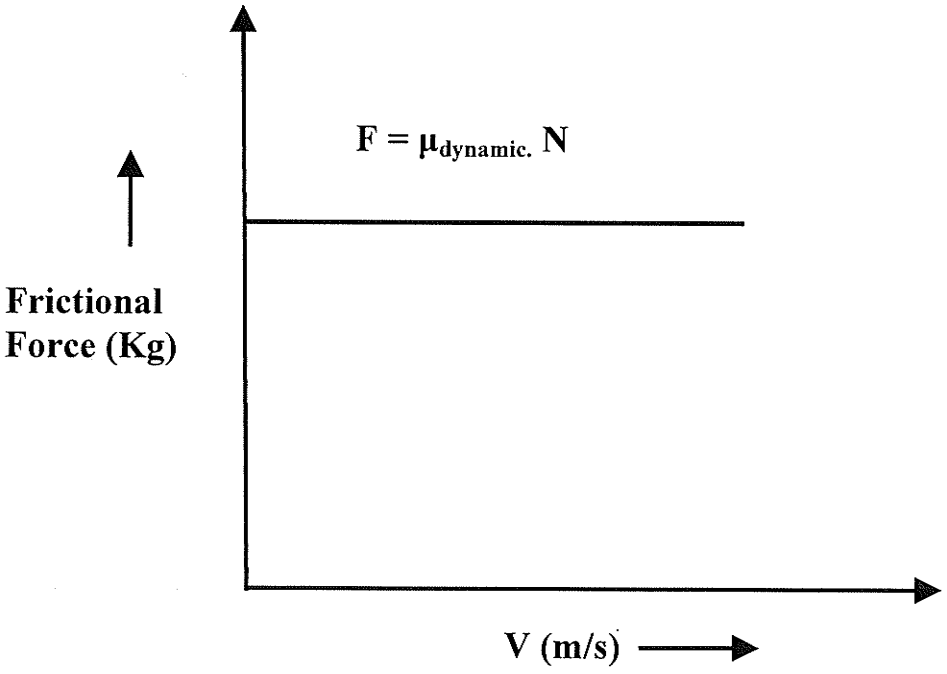

Figure A.2: An illustration of Coulomb's law

depends on the material used. If the surfaces slide past each other easily, they tends to have a low coefficient of friction, while the materials which do not slide past each other easily tends to have a higher coefficient of friction. Hence, the coefficients of friction may vary from zero to greater than one – depending on the materials used. Also, the coefficient of friction is an empirical measurement – it has to be measured experimentally, and cannot be determined through calculations

The possible causes of friction are due to interaction between the contact surfaces and this result in resistance to relative motion. Two theories have been put forward to describe the microscopic nature of the frictional contact, Bowden and Tabor [40], Halling [41] and Hutchings [43];

- adhesion theory; two surfaces adhere over some part of the contact
- deformation or displacement theory; if no adhesion takes place, then material must be deformed or displaced to accommodate the relative motion, i.e. asperity interlocking or material displacement (sometimes called macro-displacement)

Adhesion Theory

Bowden and Tabor [36] stated that when metal surfaces are pressed against each other, the adjacent asperities (microscopic peaks on the metal surface) make contact first, thus the real contact area is considerably smaller than the actual area. Since this area is substantially small, the pressure is therefore large and this causes plastic deformation at the tips of the asperities. This plastic deformation continues until the area is sufficiently large reducing the stress below the yield stress. Over these regions of intimate contact,

strong adhesion takes place between the adjacent surfaces, and 'cold welds' or junctions are developed. Obviously the force needed to break these welds is equal to the frictional force. This theory describes the first two laws of friction, that friction is independent of apparent area of contact and the friction force is proportional to the load. For two metals at atmospheric pressure, the predicted coefficient is approximately 0.2 which is somewhat lower than the observed value of 0.5.

This simple theory was modified to take into account the plastic flow as the horizontal force is applied just prior to slip. This two-dimensional model produces a principal stress direction which is the resultant of the normal asperity yield stress and the applied horizontal shear stress. The plastic flow associated with the applied shear stress causes an increase in the contact area, i.e. there is a junction growth. This increase in contact area causes the normal and horizontal stresses to decrease, thus delaying yield and pushing up the theoretical coefficient of friction.

Interacting Asperity Theory

This theory was proposed by Halling [41] by extending previously developed ideas. It has been observed that for sliding surfaces, there is macroscopic motion parallel to the contact surface. If two wedge shapes interlock, then motion can only occur if one or both plastically deform. If an assumption is made for the wedge angle, then the relative shearing and normal forces can be calculated to produce complete asperity separation. The coefficient of friction is then the sum of the instantaneous shearing forces for all contacting asperities, divided by the sum of all the normal forces for the contacting

asperities. Assuming the junction angle to be 0^{o}, an interesting situation develops where this theory predicts the same relationship as the Bowden and Tabor [40] theory. If a soft metal and hard metal are in contact, then this asperity separation is modified to produce a ploughing effect of the harder metal through the surface of the softer metal.

The energy losses in both these theories come from the plastic deformation which occurs in the asperities. Although fracture occurs in the interlocking asperity theory and it must occur in the adhesion theory, the energy losses associated with this are small in comparison to plastic deformation. It can be shown that for the fracture produced from an asperity contact, the asperity makes about 1000 other contacts where only plastic deformation occurs.

Accompanying Compact Disk (CD)

This thesis is a compound document i.e. text on paper accompanied by electronic material on a CD-ROM. The accompanying CD-ROM contains Appendix B, C and D. These files are created using in Microsoft Office Excel 2003.